

1           Age-related changes in the local milieu of inflamed tissues cause  
2 aberrant neutrophil trafficking and subsequent remote organ damage

3  
4           Anna Barkaway<sup>1</sup>, Loïc Rolas<sup>1</sup>, Régis Joulia<sup>1</sup>, Jennifer Bodkin<sup>1</sup>, Tchern Lenn<sup>1</sup>, Charlotte  
5 Owen-Woods<sup>1</sup>, Natalia Reglero-Real<sup>1</sup>, Monja Stein<sup>1</sup>, Laura Vazquez Martinez<sup>1</sup>, Tamara  
6 Girbl<sup>1</sup>, Robin N. Poston<sup>1</sup>, Matthew Golding<sup>1</sup>, Rebecca S. Saleeb<sup>1</sup>, Aude Thiriot<sup>2</sup>, Ulrich H.  
7 von Andrian<sup>2</sup>, Johan Duchene<sup>3</sup>, Mathieu-Benoit Voisin<sup>1</sup>, Cleo L. Bishop<sup>4</sup>, David Voehringer<sup>5</sup>,  
8           Axel Roers<sup>6</sup>, Antal Rot<sup>1,7</sup>, Tim Lämmermann<sup>8</sup> & Sussan Nourshargh<sup>1,7,9\*</sup>

9  
10          <sup>1</sup>Centre for Microvascular Research, William Harvey Research Institute, Barts and The  
11 London School of Medicine and Dentistry, Queen Mary University of London, London EC1M  
12 6BQ, UK.

13  
14          <sup>2</sup>Department of Immunology and HMS Center for Immune Imaging, Harvard Medical School,  
15 Boston, MA, MA 02115, USA. The Ragon Institute of MGH, MIT and  
16 Harvard, Cambridge MA 02139, USA.

17  
18          <sup>3</sup>Institute for Cardiovascular Prevention (IPEK), Ludwig-Maximilians-Universität (LMU)  
19 München, Munich 80336, Germany.

20  
21          <sup>4</sup>Centre for Cell Biology and Cutaneous Research, Blizard Institute, Barts and The London  
22 School of Medicine and Dentistry, Queen Mary University of London, London E1 2AT, UK.

23  
24          <sup>5</sup>Department of Infection Biology, University Hospital Erlangen and Friedrich-Alexander  
25 University Erlangen-Nuremberg (FAU), Erlangen 91054, Germany.

26  
27          <sup>6</sup>Institute for Immunology, Medical Faculty Carl Gustav Carus, Technische Universität  
28 Dresden, Dresden 01069, Germany.

29  
30          <sup>7</sup>Centre for Inflammation and Therapeutic Innovation, Barts and The London School of  
31 Medicine and Dentistry, Queen Mary University of London, London EC1M 6BQ, UK.

32  
33          <sup>8</sup>Max Planck Institute of Immunobiology and Epigenetics, Freiburg, Germany.

34  
35          <sup>9</sup>Lead contact

36          \*Correspondence: [s.nourshargh@gmul.ac.uk](mailto:s.nourshargh@gmul.ac.uk)

37  
38          A. Barkaway and L. Rolas contributed equally.

1 **SUMMARY**

2 Aging is associated with dysregulated immune functions. Here, we investigated the impact of  
3 age on neutrophil diapedesis. Using confocal intravital microscopy, we found that in inflamed  
4 aged tissues neutrophils exhibited a high frequency of reverse transendothelial migration  
5 (rTEM). This retrograde breaching of the endothelium by neutrophils was governed by  
6 enhanced production of the chemokine CXCL1 from mast cells that localized at endothelial  
7 cell (EC) junctions. Increased EC expression of the atypical chemokine receptor 1 (ACKR1)  
8 supported this pro-inflammatory milieu in aged venules. Accumulation of CXCL1 caused  
9 desensitization of the chemokine receptor CXCR2 on neutrophils and loss of neutrophil  
10 directional motility within EC junctions. Fluorescent tracking revealed that in aged mice,  
11 neutrophils undergoing rTEM re-entered the circulation and disseminated to the lungs where  
12 they caused vascular leakage. Thus, neutrophils stemming from a local inflammatory site  
13 contribute to remote organ damage, with implication to the dysregulated systemic  
14 inflammation associated with aging.

15

16 **Key Words**

17 Neutrophils; inflammation; chemokines; endothelium; aging; CXCR2; ACKR1; extravasation

18

19

20

21

22

23

24

25

26

27

28

1

## 2 **INTRODUCTION**

3 Aging is a high-risk factor for the onset of inflammatory conditions, especially in life-threatening  
4 pulmonary and cardiovascular disorders (Akbar and Gilroy, 2020; Ferrucci and Fabbri, 2018;  
5 Nikolich-Žugich, 2018; Robba et al., 2020; Vabret et al., 2020). Regardless of the primary  
6 insult being a pathogenic microbe or sterile injury, a significant cause of mortality and  
7 comorbidity in older patients is increased susceptibility to organ dysfunction remote from the  
8 initial inflammatory trigger. This is illustrated by the SARS-CoV-2 pandemic, as elderly patients  
9 with COVID-19 are particularly at risk of pneumonia, but also present multiple organ failure  
10 (Akbar and Gilroy, 2020; Robba et al., 2020; Vabret et al., 2020). Furthermore, damage to  
11 remote organs is a significant cause of intensive care admissions following physical trauma in  
12 older patients (Lord et al., 2014). Together, aging-associated remote organ dysfunction  
13 represents an important unmet clinical problem that requires greater mechanistic  
14 understanding.

15 Advanced age promotes immune dysregulation, a phenomenon considered to be a principal  
16 cause of ageing-associated pathologies (Akbar and Gilroy, 2020; Nikolich-Žugich, 2018; Shaw  
17 et al., 2013). The underlying basis of this is complex and linked to multiple factors, such as  
18 compromised cell-intrinsic leukocyte behaviors, changes in immune cell local  
19 microenvironments and increased circulating pro-inflammatory mediators (Nikolich-Žugich,  
20 2018; Shaw et al., 2013). While aging influences innate immunity, the associated reports are  
21 varied and many mechanistic questions remain (Nikolich-Žugich, 2018; Shaw et al., 2013).  
22 Neutrophil trafficking constitutes a crucial component of innate immunity and inflammatory  
23 disease states and studies of isolated neutrophils from aged individuals have revealed  
24 reduced chemotaxis *in vitro* (Fulop et al., 2004; Sapey et al., 2014). *In vivo*, dysregulated  
25 neutrophil trafficking in aged mice is aligned with factors such as aberrant production of  
26 systemic or local inflammatory mediators or diminished local anti-inflammatory mechanisms  
27 (Eskan et al., 2012; Gomez et al., 2007; Kulkarni et al., 2019; Nomellini et al., 2012; Nomellini  
28 et al., 2008; Wulfert et al., 2012).

29 To investigate the impact of age on the dynamics of neutrophil diapedesis, we examined  
30 neutrophil breaching of venular walls in inflamed tissues of aged mice in real-time using  
31 confocal intravital microscopy (IVM). We noted increased prevalence of transmigrating  
32 neutrophils exhibiting retrograde motility within endothelial cell (EC) junctions and re-entering  
33 the vascular lumen. Mechanistically, this neutrophil reverse transendothelial cell migration  
34 (rTEM) behavior was governed by the aged stroma (tissue) and mediated by elevated  
35 production of the chemokine CXCL1 by tissue resident mast cells. Increased expression of

1 the atypical chemokine receptor 1 (ACKR1) in aged tissues facilitated the retention of CXCL1  
2 within venular EC junctions which, in turn, induced downregulation of its cognate receptor,  
3 CXCR2, on transmigrating neutrophils. This resulted in loss of neutrophil directional motility  
4 with consequent neutrophil rTEM and re-entry of neutrophils back into the circulation. rTEM  
5 neutrophils were tracked from injured tissues to the lungs where, in aged mice, they were  
6 programmed towards an activated phenotype capable of causing tissue damage. Together,  
7 an intensified local pathway involving upregulation of mast cell-derived CXCL1 and EC ACKR1  
8 was shown to mediate age-related changes in the local inflammatory milieu that is capable of  
9 prompting noxious neutrophil re-entry into the systemic circulation, ultimately inducing  
10 downstream remote organ injury.

11

## 12 **RESULTS**

### 13 **Inflamed aged stroma promotes aberrant neutrophil transendothelial cell migration**

14 The impact of age on neutrophil-venular wall interactions was investigated in inflamed mouse  
15 cremaster muscles that due to its translucency is amenable to high resolution IVM. Cremaster  
16 muscles were acutely inflamed via local injection of IL-1 $\beta$  in young and aged mice and  
17 leukocyte responses were investigated in real-time. Analysis of tissues of wild-type (WT) mice  
18 revealed significantly enhanced leukocyte rolling and adhesion in aged ( $\geq 18$  months), as  
19 compared to young (2-4 months) mice (Figures 1A & 1B). A similar increase in leukocyte firm  
20 adhesion was observed in TNF-stimulated aged tissues (Figure S1A). Breaching of venular  
21 walls was investigated using neutrophil reporter mice *Lyz2-EGFP-ki* (display GFP<sup>bright</sup>  
22 neutrophils) and following staining of EC junctions by locally administered non-blocking anti-  
23 CD31 mAb (Woodfin et al., 2011). Young *Lyz2-EGFP-ki* mice showed a notable frequency of  
24 neutrophil TEM events, typified by full breaching of the endothelium in a luminal-to-abluminal  
25 manner, a response termed normal TEM (nTEM; Video S1). Despite exhibiting increased  
26 neutrophil-EC adhesion (Figures 1A, 1B & S1A), aged mice showed a lower number of  
27 neutrophil nTEM events (Figure 1C) and reduced neutrophil infiltration into the perivascular  
28 space (Figures 1D & 1E). These findings were accounted for by a high frequency of neutrophil  
29 retrograde motility within EC junctions (reverse TEM; rTEM) (~20% of all TEM events; Figures  
30 1F, 1G & Video S2) that led to the eventual re-entry of the neutrophils back into the vascular  
31 lumen. In line with our previous findings (Owen-Woods et al., 2020; Woodfin et al., 2011), IL-  
32 1 $\beta$ -inflamed tissues of young mice showed negligible evidence of neutrophil rTEM (Figure  
33 1G). We also observed neutrophil rTEM in IL-1 $\beta$ -stimulated ear skin of aged mice (Video S3),

1 a model that exhibited comparable levels of neutrophil rTEM in male and female animals  
2 (~12% in relation to all TEM events).

3 To investigate the relative contribution of neutrophils versus the stroma (tissue) to the  
4 observed dysregulated neutrophil TEM in aged mice, a series of bone marrow (BM) chimeric  
5 animals were established (Figure 1H). Two chimeric cohorts were generated by BM transfer  
6 from aged and young *Lyz2-EGFP-ki* mice into irradiated young and aged WT, respectively.  
7 This yielded animals with aged hematopoietic cells and young stroma (A→Y), and conversely,  
8 mice with young hematopoietic cells and aged stroma (Y→A). A control group of young  
9 irradiated WT mice received BM from young *Lyz2-EGFP-ki* mice (Y→Y). All chimeras  
10 exhibited similar blood neutrophil counts (Figure S1B) and reconstitution levels of GFP<sup>bright</sup>  
11 neutrophils (≥95%). Aged chimeras showed similar vascular, stromal and functional  
12 characteristics as compared to non-irradiated aged mice (Table S1). Whilst all chimeric mice  
13 displayed robust luminal adhesion, this was increased in Y→A chimeras (exhibiting aged  
14 stroma) as compared to A→Y and Y→Y chimeras (Figure 1I). However, Y→A chimeras  
15 displayed reduced nTEM (Figure 1J) and reduced neutrophil migration into the perivascular  
16 tissue (~43%), as compared to Y→Y control chimeric animals. Furthermore, although almost  
17 absent in Y→Y and A→Y chimeras, Y→A chimeras exhibited an increased frequency of  
18 neutrophil rTEM (~15%; Figure 1K). In line with these findings, GFP<sup>bright</sup> BM neutrophils of  
19 young donors adoptively transferred into IL-1β-stimulated WT mice displayed 21.7%  
20 neutrophil rTEM in aged recipients, while no such events were seen in young recipients (0%;  
21 n=4 mice/group). Collectively, aged mice exhibit disrupted neutrophil-EC interactions,  
22 characterized by a high frequency of neutrophil rTEM, with clear evidence of aged stroma  
23 driving this retrograde neutrophil migration.

24

### 25 **CXCL1 drives aging-associated neutrophil reverse TEM**

26 Since a heightened pro-inflammatory state is a feature of aging (Ferrucci and Fabbri, 2018;  
27 Nikolich-Zugich, 2018), we considered that aging-associated aberrant neutrophil TEM may be  
28 driven by a dysregulated local inflammatory milieu. To explore this, control (PBS) and IL-1β-  
29 stimulated tissues of young and aged mice were analyzed by a Cytokine Array and ELISA. IL-  
30 1β-stimulated tissues produced increased levels of numerous pro-inflammatory mediators  
31 (Figure 2A & S2A). Among these, the chemokine CXCL1, a potent neutrophil chemoattractant,  
32 was significantly increased in IL-1β-stimulated aged as compared to young tissues, a profile  
33 also observed in plasma (Figures 2B & 2C).

34 Hypothesizing that high levels of CXCL1 in inflamed aged tissues might cause the observed  
35 increase in neutrophil rTEM, IL-1β-stimulated chimeric mice with aged stroma (Y→A) were

1 treated with blocking anti-CXCL1 mAb or an isotype control and analyzed by confocal IVM.  
2 Anti-CXCL1 mAb treatment had no significant effect on total neutrophil TEM events ( $12.8 \pm 2.3$   
3 as compared with  $13.5 \pm 3.8$  after isotype,  $n=4-5$  mice/group), but significantly suppressed the  
4 frequency of neutrophil rTEM ( $\sim 89\%$  inhibition; Figure 2D). In contrast, an anti-CXCL2 mAb  
5 had no inhibitory effect on the frequency of neutrophil rTEM in this inflammatory model (Figure  
6 2D).

7 Next, to shed light on the mechanisms in aging-associated overproduction of CXCL1, we  
8 investigated its cellular sources. Here, we focused on tissue resident macrophages and mast  
9 cells, known to be major sources of CXCL1 in early stages of neutrophil recruitment (De Filippo  
10 et al., 2013). Immunofluorescence (IF) staining of control and IL-1 $\beta$ -stimulated cremaster  
11 muscles showed no significant difference in macrophage numbers (Figure S2C) or  
12 macrophage-associated CXCL1 in perivascular regions of young and aged tissues (Figures  
13 S2B & S2D). In contrast, numbers of mast cells were increased in aged tissues, compared to  
14 young (Figures 2E & 2F). This was consistent across multiple organs, with ear skin and  
15 peritoneal cavity of aged animals exhibiting increased mast cell numbers as compared to  
16 young tissues (Figures 2G & S2E). Furthermore, although PBS and IL-1 $\beta$ -stimulated  
17 cremaster muscles of young mice, and PBS-treated aged tissues, showed almost  
18 undetectable levels of mast cell-associated CXCL1, mast cells of inflamed aged tissues  
19 displayed  $\sim 187\%$  per cell increase in protein expression of CXCL1, relative to stimulated  
20 young tissues (Figures 2H & 2I). Since mast cells of aged mice had a significantly greater  
21 cellular and nuclear volume (Figures 2J & S2F), were more granular (Figure S2G), and  
22 exhibited increased senescence-associated- $\beta$ -galactosidase (SA- $\beta$ -gal) activity (Figure 2K),  
23 their increased CXCL1 may be due to cellular senescence, i.e. the *senescence-associated*  
24 *secretory phenotype (SASP)* (Akbar and Gilroy, 2020; Nikolich-Žugich, 2018; Shaw et al.,  
25 2013). Furthermore, mast cells residing in aged tissues displayed reduced apoptosis (Figure  
26 S2H), suggesting their high number may represent increased survival.

27 Having identified mast cells as a key cellular source of enhanced tissue-derived CXCL1, we  
28 next directly investigated their role in age-related neutrophil rTEM. We initially analyzed aged  
29 chimeric mice depleted of their cremasteric mast cells by local administration of an anti-c-kit  
30 (ACK.2) mAb (Brandt et al., 2003), which led to  $\sim 48\%$  depletion of perivascular mast cells  
31 (Figures S2I & S2J). This treatment had no impact on the total number of TEM events (Figure  
32 S2K) but significantly suppressed the frequency of neutrophil rTEM within cremasteric venules  
33 (Figure 2L) as compared to control mice. Similarly, aged mast cell deficient mice (*Mcpt5-Cre-*  
34 *R-DTA*; Figure S2L) showed comparable levels of neutrophil TEM to their aged-matched  
35 littermate controls (Figure S2M), but no neutrophil rTEM in IL-1 $\beta$ -stimulated ear skin (Figure

1 2M). Together, the results identify mast cells as a key cellular source of tissue-derived CXCL1  
2 and a major driver of neutrophil rTEM in acutely inflamed aged tissues.

3

#### 4 **ACKR1 is elevated in aged tissues and retains mast cell-derived CXCL1 at EC junctions**

5 The dynamics and directionality of neutrophil TEM is exquisitely regulated by chemokines that  
6 are locally generated and strategically presented to migrating leukocytes (Girbl et al., 2018;  
7 Nourshargh and Alon, 2014). In line with this fundamental concept, we hypothesized that  
8 excessive CXCL1 in inflamed aged tissues may promote aberrant neutrophil TEM due to its  
9 altered patterning on venular ECs. To explore, cremaster muscles of young and aged mice  
10 were analyzed for CXCL1 localization by IF and confocal microscopy. Although PBS-treated  
11 tissues exhibited an almost undetectable CXCL1 signal on ECs, this was increased with IL-  
12 1 $\beta$ -treatment (Figures 3A & S3A). In stimulated young tissues, CXCL1 was evenly distributed  
13 in ECs but inflamed aged tissues exhibited increased junctional CXCL1 (Figures 3A & 3B).  
14 Aged mice depleted of their perivascular mast cells (Figures S2I & S2J) showed significantly  
15 reduced CXCL1 localization at EC junctions, comparable to levels detected in non-junctional  
16 regions (Figure 3C).

17 Aiming to elucidate the molecular basis of mast cell-derived CXCL1 retention at EC junctions,  
18 we focused on ACKR1. This atypical chemokine receptor binds CXCL1 and numerous other  
19 chemokines with high affinity (Novitzky-Basso and Rot, 2012) and is enriched at venular EC  
20 junctions (Girbl et al., 2018; Thiriot et al., 2017). While the overall EC expression of ACKR1  
21 was increased in IL-1 $\beta$ -stimulated tissues, this response was most pronounced in aged mice  
22 (Figures 3D & 3E) that exhibited a distinct elevation in junctional localization of ACKR1  
23 (Figures 3F & 3G). In addition to ECs, ACKR1 is expressed by erythroid cells in the BM and  
24 blood where it impacts chemokine homeostasis and neutrophil phenotypes (Duchene et al.,  
25 2017). To directly investigate the functional role of EC ACKR1 in retaining endogenously  
26 generated CXCL1 at EC junctions, we generated young and aged chimeras with selective EC  
27 ACKR1 deficiency (Figures 3H, S3B, S3C & S3D). In analyzing CXCL1 expression, stimulated  
28 tissues of both young and aged EC *Ackr1*<sup>-/-</sup> chimeras showed characteristic punctate  
29 expression (Figure 3I). However, aged EC *Ackr1*<sup>-/-</sup> chimeras failed to show increased  
30 localization of CXCL1 at EC junctions (Figure 3J). While it is generally considered that  
31 erythrocyte ACKR1 governs the availability of plasma chemokines (Novitzky-Basso and Rot,  
32 2012), we detected increased plasma levels of CXCL1 in locally stimulated aged EC *Ackr1*<sup>-/-</sup>  
33 chimeras as compared to aged EC *Ackr1*<sup>+/+</sup> mice (Figure 3K). These results suggest that EC  
34 ACKR1 can control circulating levels of chemokines produced by locally inflamed tissues.

1 Collectively, inflamed aged tissues exhibit an aberrant vascular milieu characterized by an  
2 intensified expression of ACKR1 on venular ECs.

3

4

### 5 **GRK2-dependent CXCR2 downregulation promotes neutrophil rTEM in aged tissues**

6 Considering how increased retention of CXCL1 at EC junctions could influence neutrophil  
7 directional motility, we hypothesized that it might affect the expression of its cognate receptor  
8 CXCR2. IF staining showed CXCR2 expression on the plasma membrane of almost all luminal  
9 neutrophils in young tissues (Figure 4A). This was markedly reduced in aged mice, with ~30%  
10 of luminal neutrophils exhibiting low levels of membrane CXCR2 (Figures 4A). As these  
11 CXCR2<sup>lo</sup> neutrophils were almost exclusively in close proximity to EC junctions (Figure 4A),  
12 we hypothesized that this phenotype may be caused by high levels of junctional CXCL1  
13 retained by ACKR1. In addressing, we analyzed the frequency of CXCR2<sup>lo</sup> neutrophils in  
14 stimulated venules of young and aged EC ACKR1 expressing and deficient chimeras. As  
15 found in aged animals (Figure 4A), aged chimeric EC *Ackr1*<sup>+/+</sup> mice showed an increased  
16 incidence of luminal CXCR2<sup>lo</sup> neutrophils (Figure 4B). However, we detected few luminal  
17 CXCR2<sup>lo</sup> neutrophils in aged EC *Ackr1*<sup>-/-</sup> chimeras (Figure 4B). These results indicate that, in  
18 inflamed aged tissues, high levels of EC junctional ACKR1, and increased levels of CXCL1  
19 retained by it, promote downregulation of CXCR2 on transmigrating neutrophils.

20 To directly investigate the impact of reduced CXCR2 expression on neutrophil transmigration,  
21 we generated young and aged chimeric mice expressing or deficient in neutrophil G protein-  
22 coupled receptor kinase-2 (GRK2), one of a number of GRKs expressed by neutrophils known  
23 to regulate neutrophil GPCR signaling (Lämmermann and Kastenmuller, 2019). Irradiated  
24 young and aged WT recipients were injected i.v. with BM from mice with selective neutrophil  
25 GRK2 deficiency that were additionally intercrossed with *Lyz2-EGFP-ki* animals (*Mrp8-  
26 Cre;Grk2*<sup>fl/fl</sup>;*Lyz2-EGFP-ki*; Figure 4C). Control chimeras were generated through use of  
27 *Grk2*<sup>fl/fl</sup>;*Lyz2-EGFP-ki* mice as BM donors. Selective neutrophil GRK2 deficiency was  
28 confirmed using BM cells (Figure S4A) and all chimeras exhibited high levels of donor cell  
29 reconstitution in whole blood (≥95%). IL-1β-stimulated tissues of aged neutrophil *Grk2*<sup>+/+</sup>  
30 chimeras exhibited elevated levels of luminal CXCR2<sup>lo</sup> neutrophils, as compared to young  
31 *Grk2*<sup>+/+</sup> chimeras, that was reduced in aged neutrophil *Grk2*<sup>-/-</sup> mice (Figure 4D). Functionally,  
32 neutrophil GRK2 deletion had no impact on total neutrophil TEM (Figure 4E) or its duration  
33 (Figure S4B) and stimulated young neutrophil *Grk2*<sup>+/+</sup> and young neutrophil *Grk2*<sup>-/-</sup> chimeras  
34 showed almost undetectable levels of neutrophil rTEM (Figure 4F). However, while aged  
35 chimeras harboring *Grk2*<sup>+/+</sup> neutrophils exhibited a marked frequency of neutrophil rTEM, this



1 was reduced (~80% inhibition) in aged chimeras expressing *Grk2<sup>-/-</sup>* neutrophils. These results  
2 provide evidence that GRK2-mediated CXCR2 internalization induces loss of neutrophil  
3 directional motility within EC junctions of aged tissues. Collectively, in aged mice, excessive  
4 EC junctional CXCL1 elicits neutrophil CXCR2 internalization, prompting neutrophils that had  
5 initiated diapedesis to re-enter the vascular lumen.

## 6 **rTEM neutrophils stemming from locally injured aged tissues accumulate in lungs**

7 To assess the dispersion and systemic pathophysiological impact of rTEM neutrophils in aged  
8 mice, we extended our investigations to a model of local ischemia-reperfusion (IR) injury. This  
9 inflammatory insult, a hallmark of numerous aging-associated pathologies, elicited an intense  
10 neutrophil infiltration in both young and aged WT mice (Figure 5A). Since aging is associated  
11 with greater susceptibility to remote organ failure, we analyzed mice subjected to this local IR  
12 model for lung injury. Here, as indicated by increased extravascular accumulation of i.v.  
13 administered fluorescent beads (20 nm), aged mice exhibited significantly greater lung  
14 damage as compared to young at 4 h post reperfusion (Figure 5B). This response appeared  
15 to be sustained, in that notable lung permeability was detected in aged mice even at 24 h post  
16 reperfusion (~40% increase as compared to young mice; n=5 mice/group).

17 Since we have previously aligned neutrophil rTEM with distant organ damage (Colom et al.,  
18 2015; Owen-Woods et al., 2020; Woodfin et al., 2011), we next analyzed neutrophil TEM  
19 dynamics by confocal IVM. IR injury in mice expressing aged stroma (Y→A chimeras) was  
20 characterized by significant reduction in the number of nTEM events but increased frequency  
21 of neutrophil rTEM as compared to Y→Y chimeras (Figures 5C & 5D). Hypothesizing that the  
22 observed lung damage may be caused by greater frequency of rTEM neutrophils stemming  
23 from locally injured aged tissues, we assessed the dissemination of rTEM neutrophils following  
24 IR injury. For this purpose, we adapted our recently developed *in vivo* cell labelling method of  
25 tracking rTEM neutrophils, a technique that takes advantage of the strong affinity of biotin for  
26 streptavidin (Owen-Woods et al., 2020). Briefly, luminal neutrophils were stained via i.v.  
27 injection of a biotinylated anti-Ly6G mAb, followed by local application of AF647-streptavidin  
28 to inflamed tissues. Initial studies confirmed that while this strategy did not significantly label  
29 luminal neutrophils, it definitively labelled all neutrophils that had breached EC junctions during  
30 IR injury. As such, luminal neutrophils were streptavidin<sup>lo</sup>, whereas interstitial and rTEM  
31 neutrophils were streptavidin<sup>hi</sup> (Figures 5E, S5A, S5B & Video S4). With this technique, sham  
32 mice presented low levels of streptavidin<sup>hi</sup> neutrophils in blood. In contrast, IR-treated mice  
33 exhibited significant dissemination of locally generated rTEM neutrophils in the peripheral  
34 circulation at 1 h post reperfusion (Figures 5F & 5G). In line with their greater frequency of  
35 rTEM neutrophils (Figure 5D), aged animals showed an elevated level of streptavidin<sup>hi</sup>

1 neutrophils in blood (corresponding to ~5,000 and ~50,000 cells/ml of blood in young and  
2 aged animals, respectively). This response returned to baseline following 4 h reperfusion in  
3 both young and aged mice (Figure 5G), suggesting trafficking of rTEM streptavidin<sup>hi</sup>  
4 neutrophils to other organs, most likely the BM, as demonstrated previously (Owen-Woods et  
5 al., 2020). Although young mice exhibited no retention of streptavidin<sup>hi</sup> neutrophils in lungs,  
6 aged mice showed a dramatic enrichment of rTEM neutrophils in their pulmonary vasculature  
7 at 1 h post reperfusion (Figures 5H & 5I). Also evident at 4 h post reperfusion, these results  
8 suggest a sustained accumulation or retention of streptavidin<sup>hi</sup> rTEM neutrophils in the lungs  
9 of aged animals. Together, following acute local injury, aged tissues prompt a remarkable level  
10 of transmigrating neutrophils to re-enter the blood circulation, cells that disseminate to the  
11 lungs where they are retained.

12

### 13 **rTEM neutrophils are programmed towards an activated state in aged lungs and are** 14 **directly noxious to the lung tissue**

15 To directly investigate the tissue damaging potential of rTEM cells, we analyzed the phenotype  
16 of streptavidin<sup>hi</sup> rTEM neutrophils. Using blood samples collected at 1 h post reperfusion of  
17 cremasteric tissues in young and aged mice, streptavidin<sup>hi</sup> neutrophils exhibited minor  
18 phenotypic changes in both age groups, compared to streptavidin<sup>lo</sup> neutrophils (Figures S6A  
19 & S6B). These findings reflected the overall phenotype of streptavidin<sup>lo</sup> blood neutrophils that  
20 was not significantly different between sham and IR-treated groups in both young and aged  
21 mice (Figure S6C). Since we detected increased retention of streptavidin<sup>hi</sup> neutrophils in the  
22 pulmonary vasculature of aged mice (Figure 5I), we hypothesized that the pro-inflammatory  
23 state of the vasculature of aged lungs may contribute to the local tissue damaging capacity of  
24 rTEM neutrophils. To assess this, we analyzed the phenotype of pulmonary vascular  
25 streptavidin<sup>hi</sup> versus streptavidin<sup>lo</sup> neutrophils in aged animals. Here, we detected no  
26 significant phenotypic change in streptavidin<sup>hi</sup> neutrophils at 1 h post reperfusion. In contrast,  
27 streptavidin<sup>hi</sup> neutrophils of 4 h samples exhibited a marked activated state with significantly  
28 increased expression of CD11b, ICAM-1, neutrophil elastase, CD66a and CXCR4, and  
29 reduced expression of CD62L and CXCR2 (Figures 6A, 6B & 6C). These results suggest that  
30 retention of rTEM neutrophils in the pulmonary vasculature of aged mice (Figures 5H & 5I)  
31 leads to progressive activation of these cells. We detected no change in phenotype of  
32 streptavidin<sup>lo</sup> cells when comparing sham and IR groups of young and aged mice (Figure  
33 S6D). This indicates that the enhanced activation state of pulmonary neutrophils was restricted  
34 to the streptavidin<sup>hi</sup> neutrophil population, findings that are similar to those detected in blood  
35 neutrophils (see Figure S6C). Together, these data preclude the possibility that, in IR-treated

1 mice, circulating soluble factors determine the phenotype of the streptavidin<sup>hi</sup> neutrophils and  
2 show that these cells have no impact on the phenotype of streptavidin<sup>lo</sup> neutrophils.

3 Having found that rTEM neutrophils are retained and programmed towards an activated state  
4 in aged lungs, we conducted adoptive cell transfer experiments to directly investigate the  
5 potential tissue damaging impact of this scenario (Figure 6D). We FACS sorted streptavidin<sup>lo</sup>  
6 and streptavidin<sup>hi</sup> neutrophils from blood of young or aged mice subjected to IR injury at 1 h  
7 post reperfusion, cells that showed similar phenotypes and little evidence of activation (Figures  
8 S6A & S6B). The sorted cells were injected i.v. into unstimulated aged animals, and 4 or 24 h  
9 later, the mice were analyzed for multiple organ damage. Irrespective of the donor age, aged  
10 recipients injected with streptavidin<sup>hi</sup> neutrophils exhibited significantly elevated lung  
11 permeability responses at 4 h, as compared to mice injected with streptavidin<sup>lo</sup> cells (Figures  
12 6E & 6F). Assessment of lung permeability at 24 h post injection of streptavidin<sup>hi</sup> neutrophils  
13 (sorted from aged donors) indicated a sustained injury level (~31% increase in permeability;  
14 Figure 6F), suggesting limited recovery from the damage. Since streptavidin<sup>hi</sup> neutrophils were  
15 retained in the pulmonary vasculature of aged mice (Figure 5I), we hypothesized that aged  
16 tissue is the determining factor in the injurious effect of rTEM neutrophils. To test this notion,  
17 we analyzed the effect of i.v. streptavidin<sup>hi</sup> neutrophils (sorted from aged donors) in  
18 unstimulated young recipients. We saw no difference in lung permeability in mice injected i.v.  
19 with streptavidin<sup>hi</sup> neutrophils as compared to mice injected with streptavidin<sup>lo</sup> or PBS alone  
20 (Figure 6G), indicating the critical role of aged lung tissue in programming streptavidin<sup>hi</sup>  
21 neutrophils towards a noxious phenotype. We detected no change between any of the cohorts  
22 of mice with respect to permeability in the liver, heart, gut, brain or kidneys (Figure S7). Taken  
23 together, in aged animals, rTEM neutrophils constitute a population of cells that home to the  
24 lungs where they are programmed towards an activated state and are capable of directly  
25 inducing tissue damage.

26

### 27 **CXCL1 blockade protects aged mice from remote organ damage**

28 Finally, having identified increased CXCL1 in EC junctions as a driver of neutrophil rTEM in  
29 aged animals, and since rTEM neutrophils can directly cause lung damage in aged mice  
30 (Figure 6E), we considered that blockade of CXCL1 may be a strategy for protecting against  
31 aging-associated lung damage. This was investigated in the context of downstream  
32 pathological impact of local IR injury. Briefly, mice were treated i.v. with a blocking anti-CXCL1  
33 or isotype control mAb at the time of reperfusion, and were assessed for lung permeability.  
34 While following local IR, aged animals exhibited an elevated lung vascular leakage response  
35 as compared to young, this aging-associated reaction was totally abrogated with the anti-

1 CXCL1 mAb (Figure 7). These results suggest that pathways involved in driving neutrophil  
2 rTEM in aged conditions, such as dysregulated generation of directional cues, could be  
3 amenable to pharmacological blockade to protect aged individuals from developing acute lung  
4 damage post local injury.

5

## 6 **DISCUSSION**

7 Inflammation contributes to immune defenses, but when dysregulated, as is commonly  
8 observed in aging, it becomes a major detriment to normal physiological functions and health.  
9 Indeed, inflammation constitutes a major element of the aging process that is characterized  
10 by a low grade chronic inflammatory state and a shift towards increased cytokine and  
11 chemokine levels in tissues (Lopez-Otin et al., 2013; Nikolich-Žugich, 2018). The immense  
12 functional implications of this highlight the need for greater mechanistic understanding of the  
13 impact of age on immunological processes. Here, we report on the occurrence of neutrophil  
14 reverse TEM in inflamed aged tissues, an aberrant event leading to downstream remote organ  
15 injury. Mechanistically, this response was caused by a heightened inflammatory vascular  
16 milieu as elicited by defined local cellular and molecular changes. Together, we show that  
17 elucidation of deleterious mechanisms within aged tissues can identify therapeutic targets  
18 aimed at normalizing local injurious neutrophil trafficking and preventing remote organ  
19 damage in the elderly population.

20

21 Hypothesizing that aging-associated inflammation perturbs immune cell dynamics with  
22 pathological consequences, here we analyzed neutrophil trafficking *in vivo*, as investigated by  
23 high resolution confocal IVM. In aged mice, we observed a high frequency of neutrophil  
24 retrograde motility within EC junctions whereby neutrophils that had initiated diapedesis into  
25 inflamed tissues subsequently reverse migrated back to the venular lumen. Such neutrophil  
26 reverse TEM is seen *in vitro* using cultured ECs (Buckley et al., 2006), in zebra fish embryos  
27 (Mathias et al., 2006) and in certain locally inflamed mouse models (Colom et al., 2015; Owen-  
28 Woods et al., 2020; Woodfin et al., 2011). Neutrophil rTEM is aligned with downstream  
29 detrimental effects to remote organs, presenting this phenomenon as a cellular means of  
30 disseminating a local inflammatory response (Colom et al., 2015; Owen-Woods et al., 2020;  
31 Woodfin et al., 2011). As distant organ damage following local insults constitutes a significant  
32 medical problem in the elderly, the detection of increased neutrophil rTEM in aged tissues  
33 may represent a previously unknown element of aging-associated pathologies. This response  
34 was strictly driven by the aged tissue demonstrating that potential cell-intrinsic defects in  
35 neutrophil motility are unlikely to contribute to induction of rTEM. *In vitro* studies suggest

1 defective chemotaxis of neutrophils isolated from aged individuals, an effect restored by  
2 inhibition of PI3K activity (Sapey et al., 2014). Given the vital role of PI3K in neutrophil  
3 interstitial migration (de Oliveira et al., 2016), even though potential flawed neutrophil  
4 chemotaxis does not appear to compromise neutrophil TEM, it may lead to inefficient  
5 directional interstitial motility in aged tissues. In this context, neutrophil interstitial migration  
6 towards the core of an inflammatory insult is mediated by neutrophil swarming, a response  
7 choreographed by sequential phases of highly coordinated cellular behaviors, most notably  
8 chemotaxis (Kienle and Lämmermann, 2016).

9 Mechanistically, neutrophil elastase cleavage of the EC junctional adhesion molecule, JAM-  
10 C, and disrupted localized presentation of chemotactic cues are triggers of neutrophil rTEM  
11 (Colom et al., 2015; Girbl et al., 2018; Owen-Woods et al., 2020; Woodfin et al., 2011). Here,  
12 we report that induction of neutrophil rTEM within aged venules was attributed to a heightened  
13 tissue inflammatory milieu, in particular, to increased levels of the ELR<sup>+</sup> CXC chemokine,  
14 CXCL1. Among the most potent inducers of neutrophil trafficking, CXCL1 is released by  
15 stimulated vascular and perivascular cells. In this study we identified mast cells as a principal  
16 source of excessive CXCL1 and driver of neutrophil rTEM in inflamed aged tissues. The  
17 significant role of mast cells in this phenomenon appeared to be regulated at multiple levels.  
18 Aged tissues exhibited increased numbers of mast cells in close apposition to venular walls,  
19 a finding that is in agreement with data from aged human skin (Gunin et al., 2011; Pilkington  
20 et al., 2019). Mast cells of stimulated aged tissues were an abundant source of CXCL1, a  
21 cellular feature that was not evident in young tissues. Considering potential causes of this,  
22 mast cells of aged mice presented numerous elements of cellular senescence, suggesting  
23 that their enhanced capacity to generate CXCL1 may be linked to a cell type- and context-  
24 dependent SASP. The SASP represents one of a multitude of responses aligned with cellular  
25 senescence, a state of permanent cell-cycle arrest that can be induced by a range of  
26 exogenous and endogenous stresses (Franceschi and Campisi, 2014). Whilst the properties  
27 and causes of mast cell senescence require further explorations, the oxidative stress  
28 environment of aged tissues is a key inducer of senescence (Franceschi and Campisi, 2014).  
29 The SASP may also facilitate enhanced vascular permeability through increased release of  
30 mast cell-derived pro-permeability mediators (e.g. histamine and LTC<sub>4</sub>), the former being a  
31 response that aligns with induction of neutrophil rTEM (Owen-Woods et al., 2020). The pro-  
32 inflammatory state and altered structural changes of aged tissues may additionally induce  
33 exaggerated responsiveness of tissue resident cells by providing co-stimulatory signals. An  
34 example is increased levels of extracellular matrix molecules (ECMs) (Kular et al., 2014;  
35 Labat-Robert, 2004) that could prime cells for elevated effector functions, and indeed, mast  
36 cells adherent to ECMs release greater levels of pro-inflammatory mediators. Moreover,

1 ECMs may act as local cellular docking substrates (Krüger-Krasagakes et al., 1999; Oki et al.,  
2 2006), a mechanism that could contribute to increased retention and survival of mast cells and  
3 hence their increased number in aged organs.

4 Appropriate regulation of cellular dynamics within the complex 3-dimensional structures of the  
5 vascular system, lymphoid and non-lymphoid organs is a fundamental element of effective  
6 physiological immunity (Germain et al., 2012; Nourshargh and Alon, 2014; Weninger et al.,  
7 2014). In the context of neutrophil diapedesis, this is exquisitely regulated by correct spatial  
8 and temporal localization of chemokines within stimulated venular walls (Girbl et al., 2018;  
9 Nourshargh and Alon, 2014). Hypothesizing that excessive mast cell-derived CXCL1 disrupts  
10 the correct vascular localization of this chemokine, we noted enhanced presentation of CXCL1  
11 at EC junctions of aged venules. This retention was entirely mediated by ACKR1 that was  
12 expressed at elevated levels in aged post-capillary venules. While ACKR1 contributes to the  
13 regulation of chemokine availability on ECs and leukocyte diapedesis (Girbl et al., 2018;  
14 Pruenster et al., 2009), here we report that aging-associated increased protein expression of  
15 EC ACKR1 was detrimental to normal physiological neutrophil diapedesis. Specifically, EC  
16 ACKR1 played an indispensable role in retention of mast cell-derived CXCL1 at EC contacts.  
17 Additionally, it facilitated downregulation of CXCL1's cognate receptor, CXCR2, on  
18 transmigrating neutrophils. Together, these sequential events promoted neutrophil rTEM, thus  
19 identifying increased protein level of ACKR1 as a significant element of aberrant neutrophil  
20 trafficking in inflamed aged tissues. Hence, although downregulation of neutrophil GPCRs  
21 provides a physiological mechanism that fine tunes neutrophil migration and effector functions  
22 in response to surrounding stimuli, their sustained refractory state can result in dysregulated  
23 or aborted cell migration. This was illustrated *in vivo* through the use of chimeric mice  
24 expressing GRK2 deficient neutrophils. GRK2 is a G protein receptor kinase necessary for the  
25 phosphorylation and internalization of CXCR2 (Aragay et al., 1998; Raghuwanshi et al., 2012),  
26 and its deletion in neutrophils had no impact on TEM initiation indicating that pre-TEM  
27 adhesion events are not regulated by CXCR2 desensitization. However, neutrophil GRK2  
28 deficiency led to complete abolition of neutrophil rTEM in aged mice, confirming CXCR2  
29 desensitization as the causal trigger of this aberrant response. Together, our findings  
30 demonstrate that ACKR1-mediated pro-inflammatory state of aged venules instigates  
31 excessive ligation, and hence desensitization, of neutrophil CXCR2, resulting in loss of  
32 neutrophil directional motility within EC junctions.

33 Collectively, we describe a cascade of events that elicit dysregulated neutrophil migration  
34 through aged venular walls. Essential components of this are changes in the local  
35 inflammatory milieu, namely, (i) an increased number and activation state of mast cells that  
36 underpin elevated tissue levels of CXCL1, and (ii) an increased protein level of EC ACKR1.

1 As such, while the role of mast cells in innate and adaptive immunity is well acknowledged  
2 (Galli et al., 2020), our findings support the concept that these tissue-resident immune cells  
3 contribute to the pro-inflammatory state of aged tissues. Additionally, we have identified mast  
4 cells as key regulators of the dynamics of neutrophil trafficking in aging. Since mast cell  
5 numbers are increased in inflammatory disorders, such as asthma, rheumatoid arthritis and  
6 psoriasis (Siebenhaar et al., 2018), the mechanistic insights provided here may extend to  
7 chronic inflammatory conditions. With respect to ACKR1, while its expression on erythrocytes  
8 is considered as a sink or reservoir for inflammatory chemokines in the circulation and EC  
9 ACKR1 plays a crucial role in mediating leukocyte trafficking (Girbl et al., 2018; Novitzky-  
10 Basso and Rot, 2012), the mechanisms that regulate ACKR1 expression and function require  
11 further exploration. Here, since cytokine stimulation induced upregulation of EC ACKR1  
12 protein in both young and aged tissues, EC ACKR1 expression appears to be transcriptionally  
13 regulated. Furthermore, this effect is likely to be exaggerated by the heightened pro-  
14 inflammatory state of aged tissues. The mechanisms that determine junctional localization of  
15 ACKR1 however remain unexplored. Similarly to mast cell numbers, ACKR1 protein  
16 expression is increased in chronic inflammatory settings, as indicated by its upregulation on  
17 ECs in CNS microvessels during experimental and human multiple sclerosis (Minten et al.,  
18 2014). The molecular basis of the tissue aberrations reported here are likely very complex and  
19 representative of tissue-level adaptations to the pro-inflammatory stress state of aged stroma.  
20 Hence, we can speculate that altered mast cell numbers and phenotype may represent a  
21 compensation for aging-associated defective local immune and wound healing mechanisms.  
22 Similarly, increased expression of vascular ACKR1 may be a homeostatic adaptation to aging-  
23 associated exaggerated local and systemic inflammation.

24 Linking neutrophil rTEM to remote organ injury (Colom et al., 2015; Owen-Woods et al., 2020;  
25 Woodfin et al., 2011) indicates an important pathomechanistic role for this migratory response.  
26 Extending this paradigm, here we provide direct evidence for noxious capability of rTEM  
27 neutrophils and offer neutrophil rTEM as a novel mechanistic component of distant organ  
28 damage in aging. The local mechanisms linked to the induction of neutrophil rTEM are highly  
29 amenable to therapeutic targeting (e.g. involvement of CXCR2 ligands, mast cells and GRK2),  
30 and as such, present new potential opportunities of suppressing remote organ damage in  
31 elderly individuals. Although details of how rTEM neutrophils induce tissue damage remain to  
32 be determined, rTEM neutrophils retained in lungs exhibited an adhesive phenotype and  
33 expressed elevated cell surface levels of neutrophil elastase and CXCR4. These molecular  
34 changes can collectively contribute to the trafficking, enrichment and tissue destructive  
35 capability of rTEM neutrophils in lungs (Németh et al., 2020; Wang et al., 2017). As the homing  
36 and retention of rTEM neutrophils in aged lungs was instrumental in their programming

1 towards an activated state, elucidating the molecular basis of this process will be of particular  
2 interest. The lung microvasculature is a significant depot for neutrophils, supporting neutrophil-  
3 mediated host defense and immunoregulation of activated, primed and aged neutrophils  
4 (Granton et al., 2018). Aiming to delineate lung-specific recruitment mechanisms, dipeptidase-  
5 1 is a regulator of neutrophil homing to lungs (Choudhury et al., 2019), but whether the  
6 expression of this molecule is regulated by aging is unknown. Additionally, mouse single cell  
7 transcriptomic data (Consortium et al., 2018; Kalucka et al., 2020) hold immense promise in  
8 identifying organ-specific mechanisms of immune cell trafficking that can be subsequently  
9 explored in aged tissues.

10 In summary, despite the advances in neutrophil biology, and the greater understanding of the  
11 neutrophil's role in immune pathophysiology, development of therapeutic strategies aimed at  
12 suppressing neutrophil-mediated tissue damage, without compromising immunity, has made  
13 little progress. However, targeting the generation and or function of noxious neutrophil  
14 "subsets" is emerging as a plausible means of controlling neutrophil-mediated disease on-set  
15 and progression (Beyrau et al., 2012; Ng et al., 2019; Scapini et al., 2016). Here, we present  
16 evidence for neutrophils that exhibited rTEM as one such specific neutrophil subpopulation  
17 with great tissue-destructive potential. The mechanistic insights delivered by this work suggest  
18 possible therapeutic avenues for suppression of aging-associated pathologies and provide a  
19 deeper understanding of immune cell trafficking in the broader context of chronic inflammatory  
20 disorders.

21

## 22 **LIMITATIONS OF THE STUDY**

23 Having identified altered number and phenotype of mast cells as key elements of increased  
24 frequency of neutrophil rTEM in aged tissues, determining the underlying mechanisms of  
25 these cellular events will be a critical goal. Such works could involve assessing the impact of  
26 age on the number of circulating mast cell precursors and local levels of mast cell growth  
27 factors. Furthermore, while the findings of this study have immense implications for ageing-  
28 associated pathologies, at present there is no evidence for increased occurrence of neutrophil  
29 rTEM in aged individuals. To address this important limitation, defining the molecular signature  
30 of murine and human neutrophils at single cell level post exhibiting reverse TEM will be a key  
31 objective of future studies. Such works will act as a crucial prerequisite for the detection and  
32 functional evaluation of rTEM neutrophils in a broader range of physiological and pathological  
33 inflammatory settings in humans and experimental systems. Finally, establishing the  
34 molecular basis of rTEM neutrophil retention in lungs and the mechanism through which they



1 are programmed towards an activated and tissue-damaging neutrophil sub-set by genetic and  
2 pharmacological means will be critical avenues to explore.

3

4

5

## 6 **Acknowledgements**

7 This work was funded by the Wellcome Trust (098291/Z/12/Z to S.N.). Additionally, the study  
8 was supported by funds from the British Heart Foundation (PG/17/85/33395 to S.N. R.J. and  
9 M-B.V.), the People Programme (Marie Curie Actions) of the EU's 7<sup>th</sup> Framework Programme  
10 (FP7/2007-2013) under REA grant agreement (n° 608765) (to L.R., R.J., and S.N.) and the  
11 Deutsche Forschungsgemeinschaft SFB1123-A10 (to J.D.). We thank Dr T.J. Williams for  
12 critical assessment.

## 13 **Author Contributions**

14 Conceptualization and writing (first draft): A.B., L.R. and S.N.; Methodology, investigation,  
15 analysis and validation: S.N., A.B., L.R., R.J., J.B., C.O-W., T.L., T.G., M-B.V., C.L.B., N.R-  
16 R., M.S., L.V.M., M.G.; Resources: R.N.P., R.S.S., A.T., U.H.v.A., J.D., C.L.B., D.V., A.R.,  
17 A.R., T.L.; Editing of draft: All authors; Overall project conception, supervision and funding:  
18 S.N.

## 19 **Declaration of Interests**

20 The authors declare no competing interests.

21

22 **Figure 1: Inflamed aged stroma promotes aberrant neutrophil transendothelial cell**  
23 **migration. (A-G)** Young (2-4 months) and aged ( $\geq 18$  months) mice were treated intrascrotally  
24 (i.s.) with PBS or IL-1 $\beta$  and neutrophil responses in cremasteric post-capillary venules  
25 analyzed. Leukocyte **(A)** rolling flux and **(B)** firm adhesion in WT mice as quantified by  
26 brightfield IVM (n=3-16 mice/group). Neutrophil **(C)** normal TEM events (n=5-7 mice/group;  
27 Video S1), **(D)** total extravasation (n=5-7 mice/group) and **(E)** related representative images  
28 of *Lyz2-EGFP-ki* venules, as assessed by confocal IVM (scale bar: 15  $\mu$ m). **(F)** Time-lapse  
29 confocal images (Video S2) showing a neutrophil rTEM event in an IL-1 $\beta$ -stimulated aged  
30 *Lyz2-EGFP-ki* venule with the neutrophil in the sub-endothelial space (t=17 mins) re-entering

1 the vascular lumen (t=26 min to t=46 min). Top panel: *en face* luminal view; bottom panel:  
2 cross-sections; arrows: direction of neutrophil motility (scale bar: 10  $\mu$ m). (G) Frequency of  
3 neutrophil rTEM in *Lyz2-EGFP-ki* stimulated tissues (n=5-6 mice/group). (H) The generation  
4 of Y $\rightarrow$ Y, A $\rightarrow$ Y or Y $\rightarrow$ A chimeras (young 'Y'; or aged 'A') and (I-K) their analysis post treatment  
5 with i.s. PBS or IL-1 $\beta$ . Cremaster muscle (I) leukocyte firm adhesion as assessed by brightfield  
6 IVM (n=3-10 mice/group), (J) neutrophil normal TEM events (n=4-5 mice/group) and (K)  
7 frequency of neutrophil rTEM as assessed by confocal IVM (n=3-5 mice/group). Means  $\pm$   
8 SEM, #p<0.05, ##p < 0.01, ###p<0.001, ####p<0.0001 relative to aged-matched controls and  
9 \*p<0.05, \*\*p<0.01, \*\*\*p<0.001, \*\*\*\*p<0.0001, n.s. not significant, as indicated. See also Figure  
10 S1.

11

12 **Figure 2: CXCL1 drives aging-associated neutrophil reverse TEM.** (A-D) Young and aged  
13 mice were treated i.s. with PBS or IL-1 $\beta$ . (A) Inflammatory mediator analysis in homogenized  
14 cremaster muscles as assayed by protein array (n=3 mice/condition). (B) CXCL1 levels in  
15 cremaster muscles (n=4-7 mice/group) or (C) plasma (n=4-8 mice/group) as quantified by  
16 ELISA. (D) Frequency of neutrophil rTEM in Y $\rightarrow$ Y or Y $\rightarrow$ A chimeras (generated as detailed in  
17 Figure 1H) treated i.v. with isotype control, anti-CXCL1 or anti-CXCL2 blocking mAbs (n=3-5  
18 mice/group). (E) Representative confocal images of mast cells (MCs; Avidin) associated with  
19 post-capillary venules (CD31) in young and aged unstimulated WT cremaster muscles (scale  
20 bar: 20  $\mu$ m) and quantification in (F) cremaster muscles, and (G) ear skin (n=5-7 mice/group).  
21 (H-I) Analysis of CXCL1 expression in MCs of young and aged IL-1 $\beta$ -stimulated cremasteric  
22 tissues by confocal microscopy with (H) showing representative images and (I) quantification  
23 by MFI (scale bar: 5  $\mu$ m; n=3-7 mice/group). (J) Representative confocal images of MCs  
24 (CD117) in young and aged unstimulated WT ear skin (scale bar: 10  $\mu$ m) and quantification  
25 of MC volume (n=4 mice/group). (K) Peritoneal MCs acquired from unstimulated young and  
26 aged mice assayed for SA- $\beta$ -galactosidase activity by flow cytometry (n=6-13 mice/group). (L)  
27 Frequency of neutrophil rTEM in control and MC depleted IL-1 $\beta$ -stimulated cremaster muscles  
28 of aged chimeras (see Figure 1H; n=4-5 mice/group). (M) Frequency of neutrophil rTEM in IL-  
29 1 $\beta$ -stimulated ear skin of aged MC deficient (*Mcpt5-Cre-R-DTA*) mice and littermate controls  
30 (n=5 mice/group). Means  $\pm$  SEM, #p<0.05, ##p<0.01, ###p<0.001, ####p<0.0001 relative to  
31 controls, \*p<0.05, \*\*p<0.01, \*\*\*p<0.001, \*\*\*\*p<0.0001 as indicated. See also Figure S2.

32

33 **Figure 3: ACKR1 is elevated in aged tissues and retains mast cell-derived CXCL1 at EC**  
34 **junctions.** (A-G) Young and aged WT mice were treated i.s. with PBS or IL-1 $\beta$  and cremaster  
35 muscles analyzed by confocal microscopy. (A) Representative confocal images of post-

1 capillary venules (PCVs) immunostained for CD31 and CXCL1 (scale bar: 4  $\mu$ m; dashed boxes  
2 delineate magnified areas) and (B) quantification of CXCL1 expression (MFI) at EC junctional  
3 (junc.) and non-junctional (non-junc.) regions (n=6-7 mice/group). (C) EC CXCL1 expression  
4 (MFI) in control and mast cell-depleted aged cremaster tissues (n=3-5 mice/group). (D)  
5 Representative confocal images illustrating ACKR1 expression in PCVs (CD31; scale bar: 10  
6  $\mu$ m) and ACKR1 quantification (MFI) within (E) whole ECs, and EC (F) non-junctional or (G)  
7 junctional regions (n=3 mice/group). (H) Generation of EC *Ackr1*<sup>+/+</sup> and EC *Ackr1*<sup>-/-</sup> chimeras.  
8 (I-K) Young and aged chimeras as generated in (H) were treated i.s. with IL-1 $\beta$ . (I)  
9 Representative confocal images of cremasteric PCVs immunostained for CD31 and CXCL1  
10 (scale bar: 4  $\mu$ m), (J) quantification of CXCL1 expression (MFI) within EC junctional and non-  
11 junctional regions (n=3-8 mice/group) and (K) plasma CXCL1 as quantified by ELISA (n=3-8  
12 mice/group). Means  $\pm$  SEM, #p<0.05, ##p<0.01, ###p<0.001 relative to controls, \*p<0.05,  
13 \*\*p<0.01, n.s. not significant, as indicated. See also Figure S3.

14

15 **Figure 4: GRK2-dependent CXCR2 downregulation promotes neutrophil rTEM in aged**  
16 **tissues.** (A-F) Young and aged mice were treated i.s. with IL-1 $\beta$ . (A) Representative confocal  
17 images of cremasteric post-capillary venules (PCVs) of WT mice immunostained for CXCR2,  
18 MRP14 (neutrophils) and CD31. Arrows indicate CXCR2<sup>lo</sup> neutrophils (scale bar: 10  $\mu$ m;  
19 dashed boxes delineate magnified areas). (B) Percentage of luminal CXCR2<sup>lo</sup> neutrophils in  
20 cremasteric PCVs of EC *Ackr1*<sup>+/+</sup> and EC *Ackr1*<sup>-/-</sup> chimeras (n=3-5 mice/group). (C) Generation  
21 of neutrophil *Grk2*<sup>+/+</sup> and *Grk2*<sup>-/-</sup> chimeras. (D-F) Young and aged chimeras as generated in  
22 (C) were treated i.s. with IL-1 $\beta$ . (D) Percentage of luminal CXCR2<sup>lo</sup> neutrophils (n=3-4  
23 mice/group). (E) Total neutrophil TEM events and (F) frequency of neutrophil rTEM as  
24 assessed by confocal IVM (n=3-4 mice/group). Means  $\pm$  SEM #p<0.05, #####p<0.0001 as  
25 compared to young, \*p<0.05, \*\*\*p<0.001 as indicated. See also Figure S4.

26

27 **Figure 5: rTEM neutrophils stemming from locally injured aged tissues accumulate in**  
28 **the lungs.** Young and aged mice were subjected to sham or cremasteric IR injury. (A)  
29 Representative confocal images of post-capillary venules (PCVs) immunostained for CD31  
30 and MRP14 (neutrophils) in WT mice (scale bar: 20  $\mu$ m). (B) Representative confocal images  
31 and quantification of lung vascular leakage in WT mice 4 h post reperfusion (scale bar: 20  $\mu$ m;  
32 n=4-5 mice/group). (C) Neutrophil normal TEM events and (D) frequency of neutrophil rTEM  
33 in Y $\rightarrow$ Y or Y $\rightarrow$ A chimeras (see Figure 1H) as assessed by confocal IVM (n=6 mice/group).  
34 (E-I) Mice were injected i.v. with a biotinylated anti-Ly6G mAb and AF647-Strept locally  
35 applied to the cremaster muscle. (E) Time-lapse confocal IVM images (Video S4) of a

1 neutrophil rTEM event in an aged *Lyz2-EGFP-ki* cremaster muscle during IR injury illustrating  
2 that the neutrophil exhibiting rTEM is AF647-Strept<sup>hi</sup> (Top panel: *en face* luminal view; bottom  
3 panel: isolated neutrophil; scale bar: 4 μm). (F-I) Representative flow cytometry profiles and  
4 frequency of AF647-Strept<sup>hi</sup> neutrophils in (F-G) blood and (H-I) pulmonary vascular washouts  
5 in WT mice (n=4-11 mice/group). Numbers indicate the percentage of AF647-Strept<sup>hi</sup>  
6 neutrophils. Means ± SEM, #p<0.05, ###p<0.001, ####p<0.0001 as compared to age-  
7 matched controls, \*p<0.05, \*\*\*p<0.001, \*\*\*\*p<0.0001 as indicated. See also Figure S5.

8 **Figure 6: rTEM neutrophils are programmed towards an activated state in aged lungs**  
9 **and are directly noxious to the lung tissue.** (A-C) Young and aged WT mice were injected  
10 i.v. with biotinylated anti-Ly6G mAb, subjected to sham or cremasteric IR injury and AF647-  
11 Strept applied locally to the cremaster muscle. Expression levels of indicated markers on  
12 AF647-Strept<sup>hi</sup> neutrophils relative to levels on AF647-Strept<sup>lo</sup> neutrophils within the  
13 pulmonary vasculature (A) 1 h or (B) 4 h post-reperfusion (n=5-9 mice/group) and (C)  
14 representative histograms of indicated markers on pulmonary vascular neutrophils of aged  
15 mice 4 h post-reperfusion. (D) Flow cytometry sorting strategy of AF647-Strept<sup>lo</sup> and AF647-  
16 Strept<sup>hi</sup> neutrophils from whole blood of young or aged mice 1 h post-reperfusion and  
17 subsequent i.v. injection into naïve young or aged mice. (E-G) Extravasation of i.v. Evans blue  
18 in lung tissue in (E) aged recipients 4 h post i.v. injection of PBS or neutrophils sorted from  
19 young donors, (F) aged recipients 4 or 24 h post i.v. injection of neutrophils sorted from aged  
20 donors, and (G) young recipients 4 h post i.v. injection of PBS or neutrophils sorted from aged  
21 donors (n=4-7 mice/group). Means ± SEM \*p<0.05, \*\*p<0.01, \*\*\*\*p<0.0001, n.s. not significant  
22 as indicated or as compared to AF647-Strept<sup>lo</sup> neutrophils of the same group. See also Figures  
23 S6 and S7.

24

25 **Figure 7: CXCL1 blockade protects aged mice from lung injury.** (A) Representative  
26 confocal images of whole mount lung (scale bar: 20 μm) and (B) lung vascular leakage  
27 quantification in young and aged WT mice subjected to sham or cremasteric IR injury and  
28 treated with an isotype control or anti-CXCL1 blocking mAb (n=4 mice/group). Means ± SEM  
29 \*p<0.05, \*\*p<0.01 as indicated.

30

31

32

## 1 **STAR★METHODS**

### 2 **Resource availability**

#### 3 **Lead contact**

4 Further information and requests for resources and reagents should be directed and will be  
5 fulfilled by the lead contact Sussan Nourshargh (s.nourshargh@qmul.ac.uk).

#### 6 **Materials availability**

7 The supply of the following reagents and mice are subject to MTA agreements with the  
8 academics indicated in parentheses: Anti-ACKR1 mAb (Dr Ulrich H von Andrian); *Lyz2-EGFP-*  
9 *ki* mice (Dr Thomas Graf); *Mcpt5-Cre-R-DTA* (Dr Axel Roers).

#### 10 **Data and code availability**

11 This study did not generate or analyze large datasets or codes.

### 12 **Experimental models and subject details**

#### 13 **Animal experimental models**

14 Mice were used at ages described in the text ('young': 2-4 months, and 'aged': ≥16 months).  
15 Wild type (WT) C57BL/6J and C57BL/6JRj mice were purchased from Charles River  
16 laboratories (Margate, UK) and Janvier (Le Genest-Saint-Isle, France), respectively. For each  
17 experiment, WT strain-, aged and sex-matched mice were used. *Lyz2-EGFP-ki* mice were  
18 used with permission of Dr Thomas Graf (Center for Genomic Regulation and ICREA, Spain)  
19 and provided by Dr Markus Sperandio (LMU, Munich, Germany). These mice have a EGFP  
20 cDNA cassette knocked into the lysozyme M (*Lyz2*) locus to generate GFP<sup>+</sup> myeloid cells  
21 (GFP<sup>bright</sup> neutrophils, GFP<sup>dim</sup> monocytes and macrophages) and were backcrossed with  
22 C57BL/6 mice for at least 8 generations (Faust et al., 2000). *Ackr1<sup>-/-</sup>* mice were backcrossed  
23 onto a C57BL/6 background for at least 11 generations (Dawson et al., 2000). *Mrp8-Cre;*  
24 *Grk2<sup>fl/fl</sup>;Lyz2-EGFP-ki* and littermate control *Grk2<sup>fl/fl</sup>;Lyz2-EGFP-ki* mice were bred at the Max  
25 Planck Institute of Immunobiology and Epigenetics, Freiburg, Germany. *Mcpt5-Cre-R-DTA*  
26 mice were generated in the Roers laboratory as previously described (Dudeck et al., 2011).  
27 Briefly, the *Cre* recombinase is expressed under the control of the mast cell protease (*Mcpt*)  
28 5 promoter. These mice were bred with the R-DTA line (Voehringer et al., 2008), which  
29 expresses the diphtheria toxin selectively in these cells leading to the depletion of connective  
30 type tissue mast cells. All animals were group housed in individually ventilated cages under

1 specific pathogen-free (SPF) conditions and a 12 hour (h) light-dark cycle. Animals were  
2 humanely sacrificed via cervical dislocation at the end of experiments in accordance with UK  
3 Home Office regulations. Male mice were used for all studies, with the exception of some  
4 female mice used for senescence, apoptosis and ear IVM experiments. All *in vivo* experiments  
5 were conducted at the William Harvey Research Institute, Queen Mary University of London,  
6 UK under the UK legislation for animal experimentation and in agreement with the UK Home  
7 Office Animals Scientific Procedures Act 1986 (ASPA).

8

## 9 **Method details**

### 10 **Generation of bone marrow chimeric animals**

11 To generate chimeras, recipient mice were lethally irradiated with two doses of 5 Gray (Gy), 4  
12 h apart using a RadSource-2000 irradiator. Freshly isolated bone marrow from the femurs of  
13 young or aged *Lyz2-EGFP-ki* mice were transplanted into aged or young WT recipients. In  
14 similar experiments, bone marrow from WT mice was transplanted into *Ackr1<sup>-/-</sup>* or WT  
15 recipients to establish the requirement of non-hematopoietic expression of ACKR1. Mice  
16 exhibiting GRK2 deficiency in neutrophils and respective controls were generated by  
17 transferring bone marrow from *Mrp8-Cre;Grk2<sup>fl/fl</sup>;Lyz2-EGFP-ki* or *Grk2<sup>fl/fl</sup>;Lyz2-EGFP-ki*  
18 littermate controls into WT recipients. The following day,  $1.5 \times 10^6$  to  $2 \times 10^6$  donor bone  
19 marrow cells were injected i.v. into each irradiated recipient. Engraftment efficiency was  
20 assessed 4-8 weeks post irradiation by flow cytometry as described below. Generally, all mice  
21 receiving *Lyz2-EGFP-ki* bone marrow displayed  $\geq 95\%$  GFP<sup>bright</sup> neutrophils with similar  
22 neutrophil counts in peripheral blood. Bone marrow reconstitution of *Ackr1<sup>-/-</sup>* recipients was  
23 additionally determined by assessing ACKR1 expression on erythrocytes by flow cytometry.  
24 Chimeric mice were used 4-10 weeks post transplantation. Analysis of numerous relevant  
25 inflammatory, cellular and molecular parameters revealed comparable results in inflamed  
26 cremaster muscles of irradiated chimeras as compared to control non-irradiated mice (non-  
27 chimeric mice) (Table S1). Furthermore, non-irradiated and irradiated (chimeric) aged mice  
28 exhibited similar numbers of mast cells in their ear skin ( $7,023 \pm 1,001$  and  $7,430 \pm 1,555$  cells  
29 per  $\text{mm}^3$  of tissue  $\pm$  SEM, respectively, n=4 mice/group).

30

31

32

## 1 **Inflammatory response in cremaster muscles**

2 Mice were briefly anaesthetized with 3% isoflurane and injected intrascrotally (i.s.) with IL-1 $\beta$   
3 (50 ng), TNF (300 ng) or phosphate buffered saline (PBS) as vehicle control with or without  
4 fluorescent dye-conjugated anti-CD31 mAb (4  $\mu$ g, clone 390, Thermo Fischer Scientific) to  
5 label endothelial cell (EC) junctions, in a 400  $\mu$ l bolus for 2-4 h stimulation periods. For some  
6 intravital microscopy (IVM) experiments, cremasteric ischemia-reperfusion (IR) injury was  
7 induced as previously described (Colom et al., 2015; Woodfin et al., 2011), with ischemia  
8 induced in the exteriorized cremaster muscle of anaesthetized mice by the placement of two  
9 non-crushing metal clamps (Interfocus, Schwartz Micro Serrefine) at the base of the  
10 exteriorized tissue for 40 minutes (mins). Subsequently, the clamps were removed and tissue  
11 reperfusion allowed. Control sham operated mice underwent surgical procedures without  
12 induction of IR. For other experiments, ischemia was induced in a non-surgical manner by the  
13 application of two orthodontic bands around the intact testes and scrotum to occlude the  
14 vasculature for 40 mins, followed by 1-24 h of reperfusion.

15

## 16 **Inflammatory response in the ear skin**

17 Mice were anaesthetized by intramuscular injection (i.m.) of an anaesthetic mix containing  
18 ketamine and xylazine in PBS and ears were injected intradermally (i.d.) with IL-1 $\beta$  (50 ng), or  
19 PBS as vehicle control, together with fluorescently-labelled anti-CD31 mAb (4  $\mu$ g, clone 390,  
20 Thermo Fischer Scientific) to label EC junctions, within a 40  $\mu$ l bolus injection. Tissues were  
21 commonly analyzed 2-4 h later as detailed below.

22

## 23 **IF staining of whole mount tissues**

24 Cremaster muscles and ears were dissected and fixed in 4% paraformaldehyde (PFA, Sigma-  
25 Aldrich) for 15-60 mins at 4  $^{\circ}$ C. Tissues were blocked for non-specific staining and  
26 permeabilized in PBS containing 25% fetal calf serum (FCS; Thermo Fischer Scientific) and  
27 0.5% Triton X-100 (Sigma-Aldrich, 0.05% for CXCR2 staining) for 4-5 h at room temperature  
28 under gentle rotation.

29 Tissues were then incubated with unconjugated or fluorescent dye-conjugated primary  
30 antibodies in PBS containing 10% FCS overnight at 4  $^{\circ}$ C. Subsequently, tissues were  
31 incubated with species specific fluorescent dye-conjugated secondary antibodies for 3 h at  
32 room temperature in PBS containing 10% FCS. Antibody conjugation to Alexa Fluor-488, -

1 555, -647 or -Dylight 405 fluorophores was achieved using labelling kits according to  
2 manufacturers' instructions. Tissue samples were whole-mounted in PBS onto glass slides  
3 and imaged by confocal microscopy.

4

## 5 **Confocal microscopy and image analysis**

6 Immunostained post-capillary venules (diameter: 20-40  $\mu\text{m}$ ) of the cremaster muscle or ear  
7 skin were imaged using an upright Leica TCS SP5, Leica SP8 or an inverted Zeiss LSM 800  
8 laser-scanning confocal microscope equipped with argon and helium lasers (488, 561 and 633  
9 nm excitation wavelengths), a tunable white light laser or solid-state laser diodes (405, 488,  
10 561 and 640 nm excitation wavelengths), respectively. Serial Z-stacks of post-capillary  
11 venules were acquired using a dry 10x/0.3 objective lens, water dipping 20x/1.0 objective lens,  
12 oil immersion 40x/1.3 or 63x/1.4 objectives lenses. Resulting images of half vessels optically  
13 sectioned in the longitudinal orientation were reconstructed and analyzed by IMARIS  
14 software<sup>TM</sup> (Bitplane, Zurich, Switzerland). To capture fields up to 3 mm x 3 mm, tile scan  
15 acquisition was performed where necessary using 10% tile overlap; tiles were stitched and  
16 fused using the ZEN software (Zeiss, Germany). Venular ECs were identified by CD31, mast  
17 cells (MC) by avidin and/or CD117 and macrophages by CD206 and CD115. For the  
18 quantification of blood vessel density, serial Z-stacks of 8 random areas of cremaster muscles  
19 was performed using a 10x/0.3 dry objective. Using Imaris, the total tissue volume was  
20 quantified, then, using the CD31 channel and the Imaris Surface function, blood vessels were  
21 reconstructed in 3D and blood vessel volumes quantified. Vascular density was finally  
22 calculated by dividing the blood vessel volume with the whole tissue volume. Expressions of  
23 endogenous CXCL1, CD31 and ACKR1 were determined using a polyclonal anti-CXCL1  
24 antibody (Girbl et al., 2018), anti-CD31 and an anti-ACKR1 mAb (Thiriote et al., 2017),  
25 respectively. Quantification and localization of these molecules was determined by their mean  
26 fluorescence intensities (MFI) within (junctional) or outside of (non-junctional) an IMARIS  
27 generated isosurface of CD31. CXCL1 expression by MCs or macrophages was similarly  
28 determined using an isosurface generated on avidin or CD206 immunostaining, respectively.  
29 MC cellular and nuclear volumes were quantified within CD117 and DAPI isosurfaces  
30 generated on IMARIS, respectively. The number of perivascular MCs and macrophages was  
31 defined as number of cells within a 50  $\mu\text{m}$  perimeter of a post-capillary venule. Membrane  
32 CXCR2 expression was visually determined by immunostaining with an anti-CXCR2 mAb, and  
33 in mice not exhibiting *Lyz2-EGFP-ki* neutrophils, neutrophils were identified using an anti-  
34 MRP-14 Ab. CXCR2<sup>lo</sup> neutrophils were defined as neutrophils with a MFI 25% less than the  
35 average MFI of luminal neutrophils within the same image. For each molecule of interest,



1 immunoreactive protein expression was quantified from 4-12 images/tissue and expressed as  
2 MFI values minus the low background signal of tissues stained with specific isotype control  
3 antibodies.

4

#### 5 **Quantification of tissue chemokine content**

6 Cremaster muscles were homogenized in PBS containing 0.1% Triton and 1% Halt Protease  
7 and Phosphatase Inhibitor cocktail and mechanically dissociated using the Precellys24 beat-  
8 beading system (Bertin Technologies, France). The cytokine and chemokine expression  
9 profiles of these samples (pooled from 3 mice/group) were analyzed using a Mouse Cytokine  
10 Array Panel A kit (R&D Systems, Abingdon, Oxford) as per manufacturers' instructions. The  
11 CXCL1 content of these tissues was further validated by ELISA (R&D Systems; sensitivity: 2  
12 pg/ml). Chemokine content was expressed as per unit weight of tissue.

13

#### 14 **Cremaster muscle intravital microscopy**

15 Neutrophil-vessel wall interactions were analyzed in the mouse cremaster muscle  
16 microcirculation by brightfield and confocal intravital microscopy (IVM). For brightfield IVM,  
17 mice were injected i.s. with IL-1 $\beta$  (50 ng), TNF (300 ng) or PBS vehicle control for 4 h, after  
18 which the animals were terminally anaesthetized followed by surgical exteriorization of the  
19 cremaster muscle. Post exteriorization, the tissues were pinned flat onto a viewing platform of  
20 a custom made heated stage (maintaining the mouse body temperature at 37 °C) and the  
21 exteriorized muscle was kept warm and moist during surgery and the imaging period through  
22 continuous superfusion of warm Tyrode's salt solution (9.6 g/L Tyrodes salt and 12 mM  
23 NaHCO<sub>3</sub>). Post-capillary venules of 20-40  $\mu$ m in diameter were observed in real time using a  
24 63x water dipping objective on a transmitted light upright fixed stage microscope (Axioskop  
25 FS, Carl Zeiss) with a digital CMOS camera (Hamamatsu). Quantification of leukocyte rolling  
26 and firm adhesion (luminal neutrophils stationary for  $\geq$  30 seconds) responses were analyzed  
27 within multiple vessel segments (3-5) of several vessels (3-5) per mouse.

28 To assess the mode and dynamics of neutrophil migration across blood vessel walls, confocal  
29 IVM was applied to the neutrophil reporter *Lyz2-EGFP-ki* mice (Girbl et al., 2018; Woodfin et  
30 al., 2011). For some experiments, chimeric mice generated through transfer of *Lyz2-EGFP-ki*  
31 bone marrow to recipient animals were used. In other experiments, C57BL6/JRj mice were  
32 injected i.v. with  $1.5 \times 10^7$  bone marrow cells from young *Lyz2-EGFP-ki* donors immediately  
33 before exteriorization of the cremaster muscle. For these studies, mice were anaesthetized

1 using 3% isoflurane, and cremaster muscles stimulated via i.s. injection of IL-1 $\beta$  (50 ng), or  
2 were treated with PBS vehicle control. Concomitantly, the mice were injected i.s. with Alexa-  
3 Fluor 555-anti-CD31 mAb (4  $\mu$ g, clone 390, Thermo Fischer Scientific) to label EC junctions,  
4 all for 2 h test periods. Alternatively, mice were subjected to cremasteric IR injury as described  
5 above and as previously detailed (Woodfin et al., 2011). Mice were then terminally  
6 anaesthetized by intraperitoneal (i.p.) administration of ketamine (100 mg/kg) and xylazine (10  
7 mg/kg), and anesthesia maintained by i.m. injections of the same compounds. For IR  
8 experiments, the blood flow of the exteriorized muscle was occluded for 40 mins by the  
9 placement of two non-crushing clamps to the base of the tissue 2 h after i.s. Alexa-Fluor 555  
10 anti-CD31 mAb administration. In some experiments, blocking antibodies to CXCL1, CXCL2  
11 or isotype control mAbs (1 mg/kg; i.v.) were injected via a tail vein cannula 5 mins into the  
12 image acquisition period. In some experiments, mice were subjected to local MC depletion  
13 protocols prior to imaging as described below. To label and track rTEM neutrophils during  
14 cremasteric IR injury, biotinylated-anti-Ly6G mAb (2  $\mu$ g; i.v.) was injected 10 mins prior to the  
15 induction of ischemia. At the onset of reperfusion, the cremaster muscle was superfused with  
16 Alexa Fluor-647-streptavidin (1  $\mu$ g/ml in Tyrode's solution) for the entirety of the imaging  
17 period. Post-capillary venules with diameters of 20-40  $\mu$ m were imaged for 1-2 h using an  
18 upright Leica SP5 or SP8 confocal laser scanning microscope, both equipped with a 20x/1.0  
19 water-dipping objective lens. Using the 8,000 Hertz (Hz) resonant Z-scanner, Z-stacks of 0.7  
20  $\mu$ m optical sections were acquired at 1 min intervals. Typically, images were acquired as 300  
21 x 130 x 35  $\mu$ m segments, resulting in a voxel size of approximately 0.29 (x) x 0.29 (y) x 0.69  
22 (z)  $\mu$ m. Image series were then assembled into videos using IMARIS software to show  
23 longitudinally sectioned 'half' vessels for clarity and to enable direct visualization of luminal  
24 neutrophil-endothelial cell interactions. The mode and dynamics of neutrophil migration was  
25 determined by manual tracking of individual neutrophils using IMARIS. Normal neutrophil TEM  
26 (nTEM) was defined as a TEM event during which neutrophils fully breached EC junctions in  
27 a luminal-to-abluminal manner without pause. Neutrophil reverse TEM (rTEM) was classified  
28 as a response whereby neutrophils engaged with EC junctions, and after partial or full TEM,  
29 the cell retracted, exhibited retrograde motility and ultimately re-entered the vascular lumen.  
30 Neutrophil normal and reverse TEM events were quantified over an observation period of 60-  
31 120 mins with the latter being expressed as a percentage of total TEM events observed during  
32 the same period. Neutrophil extravasation into the interstitium per field of view was quantified  
33 by manual counting at the end of the IVM imaging period.

34

35

## 1 **Ear skin multiphoton intravital microscopy**

2 Neutrophil-vessel wall interactions were analyzed in the mouse ear skin microcirculation by  
3 multiphoton intravital microscopy (IVM), as supported by the CMR Advanced Bio-imaging  
4 Facility at QMUL. Mice were briefly anaesthetized by i.m. injection of anaesthetic mix  
5 (ketamine and xylazine in PBS) and ears were injected with i.d. IL-1 $\beta$  (50 ng) and Alexa-Fluor  
6 488-anti-CD31 mAb (4  $\mu$ g, clone 390, Thermo Fischer Scientific) in a 40  $\mu$ l bolus for a 2 h  
7 stimulation period. Thirty minutes before imaging, mice were injected i.v. with Alexa-Fluor 647  
8 anti-Ly6G mAb (1.5  $\mu$ g, clone 1A8) to label luminal neutrophils. Mice were terminally  
9 anaesthetized and the ear skin pinned out flat onto a viewing platform of a custom made  
10 heated stage (maintaining the mouse body temperature at 37 °C) such that the ventral side of  
11 the ear was imaged. The ear skin was kept warm and moist during the imaging period by  
12 continuous superfusion of warm Tyrode's salt solution (9.6 g/L Tyrodes salt and 12 mM  
13 NaHCO<sub>3</sub>). Post-capillary venules with diameters of 20-40  $\mu$ m were imaged for 1-2 h using a  
14 Leica SP8 DIVE multiphoton microscope using a 25x/1.0 IRAPO water dipping objective.  
15 Tunable 680-1300 nm infrared pulsed solid state laser (SpectraPhysics) was used at an  
16 excitation wavelength of 790 nm and detection using non-descanned and tunable PMT and  
17 HyD 4Tune(TM) detectors (AF488 detection: 496-576nm, AF647 detection: 627-707nm). Z-  
18 stacks of 0.5  $\mu$ m were acquired at 1 min intervals using the 8,000 Hz resonant Z-scanner  
19 mode. Typically, images were acquired at a size of 300 x 130 x 50  $\mu$ m with a voxel size of  
20 approximately 0.3 (x) x 0.3 (y) x 0.5 (z)  $\mu$ m. The mode and dynamics of neutrophil migration  
21 was determined by manual tracking of individual neutrophils using IMARIS image analysis  
22 software, as described above.

23

## 24 **Remote organ vascular leakage quantification**

25 Lung vascular leakage was quantified as described previously (Owen-Woods et al., 2020).  
26 Briefly, mice were subjected to non-invasive IR injury of the cremaster muscle as described  
27 above, and upon band removal, for some experiments, an IgG2a isotype control or anti-  
28 CXCL1 mAb (1 mg/kg) was injected i.v. Mice were subjected to either 4 h or 24 h reperfusion  
29 and two hours prior to culling, were injected i.v. with red (580-605) 20 nm microspheres (0.8  
30  $\mu$ l/g body weight) and Alexa-Fluor 488 conjugated anti-CD31 mAb (6  $\mu$ g) to assess vascular  
31 permeability and label the vasculature, respectively. Mice were culled by cervical dislocation,  
32 exsanguinated and a thoracotomy performed to expose the heart and lungs. The descending  
33 vena cava was clamped, and a 25G needle attached to a 10 ml syringe containing ice cold  
34 2% PFA in PBS was inserted into the right ventricle. The pulmonary vasculature was perfusion  
35 fixed at a flow rate of 1 ml/min using a syringe pump. The lung lobes were dissected from the

1 animal, and placed whole mount onto a cover slip, and imaged immediately using an inverted  
2 Zeiss LSM 800 (Carl Zeiss) confocal laser scanning microscope. Serial Z-stacks were  
3 acquired with an oil immersion 40x/1.3 objective lens at a resolution of 0.156 x 0.156 x 0.3 µm  
4 (x, y and z respectively). Images were reconstructed in 3D offline using IMARIS. Microsphere  
5 leakage into the alveolar space was quantified as MFI of microspheres outside of a CD31  
6 isosurface generated using the IMARIS software tool. MFI values were quantified from 6-10  
7 images per tissue from multiple lung lobes.

8 In some experiments, remote organ vascular permeability was quantified by accumulation of  
9 the plasma protein tracer Evans blue. Here, Evans blue solution 1% (w/v in PBS) was injected  
10 i.v. (5 µl/g body weight) 30 mins prior to sacrifice by exsanguination followed by a whole body  
11 vascular washout using 10 ml PBS. Organs were collected and tissue accumulated dye was  
12 quantified by eluting in 300 µl of formamide for 18 h at 56 °C. Optical density (OD) readings  
13 taken at 620 nm were normalized to formamide alone and used as a measure of Evans blue  
14 extravasation.

15

## 16 **Flow cytometry**

17 The level of bone marrow cell engraftment in chimeric mice, MC senescence and apoptosis,  
18 neutrophil and red blood cell phenotyping were assessed by flow cytometry. When necessary,  
19 samples were incubated with ACK erythrocyte lysis buffer (150 mM NH<sub>3</sub>Cl, 1 mM KHCO<sub>3</sub> and  
20 1 mM EDTA) for 3 to 5 mins. Samples were then washed and incubated in staining buffer (2  
21 mM EDTA and 0.5% BSA in PBS) and then incubated with anti-CD16/CD32 antibodies (5  
22 µg/ml) for 15 min at 4 °C to block Fc receptor-mediated antibody binding. Finally, samples  
23 were stained with primary antibodies directly conjugated with appropriate fluorophores at 4 °C  
24 for 30 min. Briefly, following doublet exclusion, live cell populations were gated as follows:  
25 CD45<sup>+</sup> Ly6G<sup>+</sup> CD115<sup>-</sup> (neutrophils), CD45<sup>+</sup> CD117<sup>+</sup> FCεR1<sup>+</sup> (MC) and Ter119<sup>+</sup> (erythrocytes).  
26 Accurate cells counts were validated using 123count eBeads Counting Beads (ThermoFisher  
27 Scientific) and analyzed using a LSR Fortessa flow cytometer (BD Biosciences) and FlowJo  
28 software (TreeStar).

29

## 30 **Tracking and phenotyping of rTEM neutrophils**

31 Peripheral dissemination of rTEM neutrophils away from cremaster muscles was achieved by  
32 tracking the cells as previously described (Owen-Woods et al., 2020). Briefly, naïve mice were  
33 injected i.v. with biotin anti-Ly6G mAb (2 µg), and 10 mins later, mice were subjected to non-

1 invasive cremasteric ischemia for 40 mins via the application of two orthodontic bands to the  
2 intact testes and scrotum. Upon reperfusion, mice received a local i.s. injection of AF647-  
3 streptavidin (1 µg) for 1-4 h. Whole blood was collected in PBS containing 50 mM EDTA via  
4 the inferior vena cava, and lung vascular washout was collected as previously described  
5 (Colom et al., 2015; Woodfin et al., 2011). Briefly, pulmonary vascular neutrophils were  
6 obtained via the flushing of the pulmonary vasculature. For this purpose, the descending vena  
7 cava and the aorta were clamped, the vasculature perfused with 10 mL of wash buffer (2mM  
8 EDTA and 0.5% BSA in PBS) via the right atrium and pulmonary vascular washout was  
9 collected via the left ventricle. Samples were then prepared for analysis of neutrophil  
10 populations as described in the flow cytometry section. For some experiments, neutrophils  
11 were sorted by flow cytometry into streptavidin<sup>lo</sup> and streptavidin<sup>hi</sup> populations from the whole  
12 blood of young or aged mice subjected to IR injury as described above and these purified  
13 neutrophils (≥ 99%) were then injected i.v. (~2500-3800 cells per mouse) into naïve aged or  
14 young WT recipients for 4 or 24 h prior to assessment of distant organ damage by quantifying  
15 local extravasation of i.v. Evans blue.

16

### 17 **Neutrophil GRK2 protein expression analysis**

18 Neutrophils were isolated from bone marrow of *Mrp8-Cre;Grk2<sup>fl/fl</sup>;Lyz2-EGFP-ki* or  
19 *Grk2<sup>fl/fl</sup>;Lyz2-EGFP-ki* mice using a neutrophil isolation kit (Miltenyi Biotec) according to the  
20 manufacturer's instructions. Pure neutrophil (>95% as assayed by flow cytometry) and non-  
21 neutrophil populations were collected for GRK2 protein expression by western blot. Cells were  
22 lysed in 1x Laemmli Buffer, denatured at 95 °C for 5 mins and subjected to standard Western  
23 Blot analysis using an anti-GRK2 primary mAb (Genetex) and a horseradish peroxidase-  
24 conjugated secondary Ab (Dako). Proteins were visualized by enhanced chemiluminescence  
25 acquired on a c600 camera (Azure Biosystems).

26

### 27 **Mast cell depletion**

28 Depletion of cremasteric MCs was achieved through the use of an anti-c-kit mAb by adapting  
29 previous protocols (Brandt et al., 2003). Briefly, mice were injected a total of 850 µg per mouse  
30 of the anti-c-kit mAb ACK.2 or isotype control in a series of i.p. and i.s. injections over a 7 day  
31 period. Typically, on day 1, mice were injected i.p. with 250 µg mAb, followed by daily i.s.  
32 injections of 150 µg mAb on days 2-5. Experimentation and assessment of MC depletion

1 efficiency was assessed by avidin staining and confocal microscopy of cremaster muscles on  
2 day 7.

3

#### 4 **Mast cell collection and analysis**

5 Murine MCs were harvested by peritoneal lavage as follows: naïve mice were sacrificed by  
6 cervical dislocation and 5 mL of lavage buffer (2 mM EDTA, 0.25% BSA in PBS) was injected  
7 into the peritoneal cavity and incubated for 3 min prior to collection. MCs were identified within  
8 the harvested cell suspension as described in the flow cytometry section using a LSR Fortessa  
9 flow cytometer (BD Biosciences) and FlowJo software (TreeStar) and subsequent parameters  
10 were analyzed. To quantify MC senescence, cells were incubated in suspension in OptiMEM  
11 buffer (ThermoFisher Scientific) containing 100 nM of Bafilomycin (ThermoFisher Scientific)  
12 for 1 h at 37 °C in order to increase the intracellular pH. The cell suspensions were then  
13 supplemented with 33 µM of C<sub>12</sub>FDG (ThermoFischer Scientific) for 2 h prior to analysis of  
14 C<sub>12</sub>FDG MFI. MC apoptosis was assessed as previously described (Asai et al., 2001). Briefly,  
15 peritoneal cells were stained with fluorescently-labelled primary mAbs as described in the flow  
16 cytometry section and incubated with 500 µl of Annexin V binding buffer (140 mM NaCl, 2.5  
17 mM CaCl<sub>2</sub> and 10 mM HEPES at pH 7.4) containing 5 µl of FITC-Annexin V (BD) and 5 µl of  
18 propidium iodide (Biolegend) for 15 mins. Apoptotic cells were defined as Annexin-  
19 V<sup>+</sup>/Propidium iodide<sup>-</sup>. MC granularity was assessed using the flow cytometric side scatter  
20 profile.

21

#### 22 **Quantification and Statistical analysis**

23 Data analysis was performed using Prism software (GraphPad). All data are expressed as  
24 mean ± SEM and exact n numbers for each data set are detailed in the figure legends.  
25 Differences between two groups were assessed for statistical significance using two-tailed  
26 paired/unpaired student *t* tests or Fischers exact test as appropriate. One way or two way  
27 ANOVA with Tukey, Dunnett or Holm Sidak post hoc tests were performed for multiple group  
28 comparisons as appropriate. Data were classed as statistically significant when p<0.05.

29

30

1 **Video S1 (related to Figure 1): Neutrophil normal transendothelial migration (TEM) in**  
2 **an IL-1 $\beta$ -stimulated cremaster muscle venule.**

3 The confocal IVM movie shows a cremaster muscle post-capillary venule during IL-1 $\beta$ -induced  
4 inflammation of a young *Lyz2-EGFP-ki* mouse exhibiting GFP<sup>bright</sup> neutrophils. EC junctions  
5 were stained *in vivo* with an AF555-anti-CD31 mAb (magenta). The video shows luminal and  
6 abluminal views of the transmigrating neutrophil in high optical magnification undergoing  
7 normal TEM. Here, a single neutrophil (green) breaches the endothelium (magenta) in a  
8 luminal to abluminal manner into the subendothelial space, and then the interstitial tissue. The  
9 single neutrophil was isolated from other GFP<sup>bright</sup> neutrophils for clarity by using the isosurface  
10 tool on Imaris software. The video shows a 19 min time frame.

11

12 **Video S2 (related to Figure 1): Neutrophil reverse transendothelial migration (rTEM) in**  
13 **an aged IL-1 $\beta$ -stimulated cremaster muscle venule.**

14 The video shows an IL-1 $\beta$ -stimulated cremasteric venule of an aged *Lyz2-EGFP-ki* mouse  
15 (GFP<sup>bright</sup> neutrophils). EC junctions were stained *in vivo* with an AF555-anti-CD31 mAb  
16 (magenta). The video shows a neutrophil (green) undergoing luminal to abluminal migration  
17 into the subendothelial space. Next, the neutrophil sends protrusions back into the lumen of  
18 the vessel, before fully migrating in an abluminal to luminal direction back into the vascular  
19 lumen. The single neutrophil was isolated from other GFP<sup>bright</sup> neutrophils for clarity by using  
20 the isosurface tool on Imaris software. The video shows a 45 min time frame.

21

22 **Video S3 (related to Figures 1 & 2): Neutrophil reverse transendothelial migration**  
23 **(rTEM) in aged IL-1 $\beta$ -stimulated ear skin venule.**

24 The multiphoton IVM movie shows an IL-1 $\beta$ -stimulated ear skin venule of an aged WT mouse.  
25 EC junctions were stained *in vivo* with an AF488-anti-CD31 mAb (magenta) and neutrophils  
26 (green) were visualized via the intravenous administration of an AF647-anti-Ly6G mAb. The  
27 video initially shows a neutrophil with a significant portion of its body in the sub-endothelial  
28 space. Subsequently, the neutrophil undergoes rTEM by retracting its body and fully migrating  
29 back into the vascular lumen. The single neutrophil was isolated from other AF647-Ly6G  
30 labelled neutrophils for clarity by using the isosurface tool on Imaris software. The video shows  
31 a 4 min time frame.

32

1 **Video S4 (related to Figure 5): Labelling of reverse TEM neutrophils using a novel**  
2 **biotin-streptavidin method.**

3 The confocal IVM movie illustrates a cremasteric post-capillary venule of an aged Y→A (see  
4 Figure 1H) chimeric mouse during the reperfusion phase of IR injury. EC junctions were  
5 stained *in vivo* with an AF555-anti-CD31 mAb (green). The movie illustrates a GFP<sup>bright</sup>  
6 neutrophil (blue) in the subendothelial space exhibiting AF647-Streptavidin<sup>hi</sup> (pink)  
7 fluorescence. Subsequently, the neutrophil sends protrusions back into the vessel lumen, and  
8 fully reverse migrates back to the luminal side of the vessel, and efficiently remains AF647-  
9 Streptavidin<sup>hi</sup>. The single neutrophil was isolated from other GFP<sup>bright</sup> neutrophils for clarity  
10 using the isosurface tool on Imaris software. The video shows a 32 min time frame.

11

12 **Table S1 (related to Figure 1): Functional, stromal and vascular features of IL-1 $\beta$ -**  
13 **stimulated cremaster muscles of irradiated (chimeric), as compared to non-irradiated,**  
14 **aged mice.**

15 Aged chimeric and non-chimeric mice were treated i.s. with IL-1 $\beta$  and cremaster muscles were  
16 labelled with AF555-anti-CD31 mAb. <sup>a</sup> Neutrophil migration responses in 300  $\mu$ m sections of  
17 cremasteric post-capillary venules as analyzed by brightfield or confocal IVM (n=3-8  
18 mice/group). <sup>b</sup> Stromal and vascular parameters were analyzed and quantified by confocal  
19 microscopy post staining of tissues with AF647-ACKR1, AF647-CXCL1 or AF532-Avidin (n=5-  
20 8 mice/group). Details of the quantification methods are outlined in relevant Method sections  
21 below. TEM: Transendothelial cell migration; rTEM: Reverse TEM; EC: Endothelial cell.

22

23

24

25

26

27

28



1

2 **REFERENCES**

3 Akbar, A.N., and Gilroy, D.W. (2020). Aging immunity may exacerbate COVID-19. *Science*  
4 *369*, 256-257.

5

6 Aragay, A.M., Ruiz-Gómez, A., Penela, P., Sarnago, S., Elorza, A., Jiménez-Sainz, M.C., and  
7 Mayor, F. (1998). G protein-coupled receptor kinase 2 (GRK2): mechanisms of regulation and  
8 physiological functions. *FEBS Lett* *430*, 37-40.

9

10 Asai, K., Kitaura, J., Kawakami, Y., Yamagata, N., Tsai, M., Carbone, D.P., Liu, F.T., Galli,  
11 S.J., and Kawakami, T. (2001). Regulation of mast cell survival by IgE. *Immunity* *14*, 791-800.

12

13 Beyrau, M., Bodkin, J.V., and Nourshargh, S. (2012). Neutrophil heterogeneity in health and  
14 disease: a revitalized avenue in inflammation and immunity. *Open Biol* *2*, 120134.

15

16 Brandt, E.B., Strait, R.T., Hershko, D., Wang, Q., Muntel, E.E., Scribner, T.A., Zimmermann,  
17 N., Finkelman, F.D., and Rothenberg, M.E. (2003). Mast cells are required for experimental  
18 oral allergen-induced diarrhea. *J Clin Invest* *112*, 1666-1677.

19

20 Buckley, C.D., Ross, E.A., McGettrick, H.M., Osborne, C.E., Haworth, O., Schmutz, C., Stone,  
21 P.C., Salmon, M., Matharu, N.M., Vohra, R.K., *et al.* (2006). Identification of a phenotypically  
22 and functionally distinct population of long-lived neutrophils in a model of reverse endothelial  
23 migration. *J Leukoc Biol* *79*, 303-311.

24

25 Choudhury, S.R., Babes, L., Rahn, J.J., Ahn, B.Y., Goring, K.R., King, J.C., Lau, A., Petri, B.,  
26 Hao, X., Chojnacki, A.K., *et al.* (2019). Dipeptidase-1 Is an Adhesion Receptor for Neutrophil  
27 Recruitment in Lungs and Liver. *Cell* *178*, 1205-1221.e1217.

28

29 Colom, B., Bodkin, J.V., Beyrau, M., Woodfin, A., Ody, C., Rourke, C., Chavakis, T., Brohi, K.,  
30 Imhof, B.A., and Nourshargh, S. (2015). Leukotriene B4-Neutrophil Elastase Axis Drives  
31 Neutrophil Reverse Transendothelial Cell Migration In Vivo. *Immunity* *42*, 1075-1086.

32

33 Consortium, T.M., coordination, O., coordination, L., processing, O.c.a., sequencing, L.p.a.,  
34 analysis, C.d., annotation, C.t., group, W., group, S.t.w., and investigators, P. (2018). Single-  
35 cell transcriptomics of 20 mouse organs creates a Tabula Muris. *Nature* *562*, 367-372.

36

37 Dawson, T.C., Lentsch, A.B., Wang, Z., Cowhig, J.E., Rot, A., Maeda, N., and Peiper, S.C.  
38 (2000). Exaggerated response to endotoxin in mice lacking the Duffy antigen/receptor for  
39 chemokines (DARC). *Blood* *96*, 1681-1684.

40

41 De Filippo, K., Dudeck, A., Hasenberg, M., Nye, E., van Rooijen, N., Hartmann, K., Gunzer,  
42 M., Roers, A., and Hogg, N. (2013). Mast cell and macrophage chemokines CXCL1/CXCL2  
43 control the early stage of neutrophil recruitment during tissue inflammation. *Blood* *121*, 4930-  
44 4937.

45

46 de Oliveira, S., Rosowski, E.E., and Huttenlocher, A. (2016). Neutrophil migration in infection  
47 and wound repair: going forward in reverse. *Nat Rev Immunol* *16*, 378-391.

48

49 Duchene, J., Novitzky-Basso, I., Thiriot, A., Casanova-Acebes, M., Bianchini, M., Etheridge,  
50 S.L., Hub, E., Nitz, K., Artinger, K., Eller, K., *et al.* (2017). Atypical chemokine receptor 1 on  
51 nucleated erythroid cells regulates hematopoiesis. *Nat Immunol* *18*, 753-761.

1  
2 Dudeck, A., Dudeck, J., Scholten, J., Petzold, A., Surianarayanan, S., Kohler, A., Peschke,  
3 K., Vohringer, D., Waskow, C., Krieg, T., *et al.* (2011). Mast cells are key promoters of contact  
4 allergy that mediate the adjuvant effects of haptens. *Immunity* 34, 973-984.  
5  
6 Eskin, M.A., Jotwani, R., Abe, T., Chmelar, J., Lim, J.H., Liang, S., Ciero, P.A., Krauss, J.L.,  
7 Li, F., Rauner, M., *et al.* (2012). The leukocyte integrin antagonist Del-1 inhibits IL-17-mediated  
8 inflammatory bone loss. *Nat Immunol* 13, 465-473.  
9  
10 Faust, N., Varas, F., Kelly, L.M., Heck, S., and Graf, T. (2000). Insertion of enhanced green  
11 fluorescent protein into the lysozyme gene creates mice with green fluorescent granulocytes  
12 and macrophages. *Blood* 96, 719-726.  
13  
14 Ferrucci, L., and Fabbri, E. (2018). Inflammageing: chronic inflammation in ageing,  
15 cardiovascular disease, and frailty. *Nat Rev Cardiol* 15, 505-522.  
16  
17 Franceschi, C., and Campisi, J. (2014). Chronic inflammation (inflammaging) and its potential  
18 contribution to age-associated diseases. *J Gerontol A Biol Sci Med Sci* 69 *Suppl* 1, S4-9.  
19  
20 Fulop, T., Larbi, A., Douziech, N., Fortin, C., Guerard, K.P., Lesur, O., Khalil, A., and Dupuis,  
21 G. (2004). Signal transduction and functional changes in neutrophils with aging. *Aging Cell* 3,  
22 217-226.  
23  
24 Galli, S.J., Gaudenzio, N., and Tsai, M. (2020). Mast Cells in Inflammation and Disease:  
25 Recent Progress and Ongoing Concerns. *Annu Rev Immunol* 38, 49-77.  
26  
27 Germain, R.N., Robey, E.A., and Cahalan, M.D. (2012). A decade of imaging cellular motility  
28 and interaction dynamics in the immune system. *Science* 336, 1676-1681.  
29  
30 Girbl, T., Lenn, T., Perez, L., Rolas, L., Barkaway, A., Thiriot, A., Del Fresno, C., Lynam, E.,  
31 Hub, E., Thelen, M., *et al.* (2018). Distinct Compartmentalization of the Chemokines CXCL1  
32 and CXCL2 and the Atypical Receptor ACKR1 Determine Discrete Stages of Neutrophil  
33 Diapedesis. *Immunity* 49, 1062-1076 e1066.  
34  
35 Gomez, C.R., Hirano, S., Cutro, B.T., Birjandi, S., Baila, H., Nomellini, V., and Kovacs, E.J.  
36 (2007). Advanced age exacerbates the pulmonary inflammatory response after  
37 lipopolysaccharide exposure. *Crit Care Med* 35, 246-251.  
38  
39 Granton, E., Kim, J.H., Podstawka, J., and Yipp, B.G. (2018). The Lung Microvasculature Is a  
40 Functional Immune Niche. *Trends Immunol* 39, 890-899.  
41  
42 Gunin, A.G., Kornilova, N.K., Vasilieva, O.V., and Petrov, V.V. (2011). Age-related changes  
43 in proliferation, the numbers of mast cells, eosinophils, and cd45-positive cells in human  
44 dermis. *J Gerontol A Biol Sci Med Sci* 66, 385-392.  
45  
46 Kalucka, J., de Rooij, L.P.M.H., Goveia, J., Rohlenova, K., Dumas, S.J., Meta, E., Conchinha,  
47 N.V., Taverna, F., Teuwen, L.A., Veys, K., *et al.* (2020). Single-Cell Transcriptome Atlas of  
48 Murine Endothelial Cells. *Cell* 180, 764-779.e720.  
49  
50 Kienle, K., and Lämmermann, T. (2016). Neutrophil swarming: an essential process of the  
51 neutrophil tissue response. *Immunol Rev* 273, 76-93.  
52  
53 Krüger-Krasagakes, S., Grützkau, A., Krasagakis, K., Hoffmann, S., and Henz, B.M. (1999).  
54 Adhesion of human mast cells to extracellular matrix provides a co-stimulatory signal for  
55 cytokine production. *Immunology* 98, 253-257.

1  
2 Kular, J.K., Basu, S., and Sharma, R.I. (2014). The extracellular matrix: Structure,  
3 composition, age-related differences, tools for analysis and applications for tissue  
4 engineering. *J Tissue Eng* 5, 2041731414557112.  
5  
6 Kulkarni, U., Zemans, R.L., Smith, C.A., Wood, S.C., Deng, J.C., and Goldstein, D.R. (2019).  
7 Excessive neutrophil levels in the lung underlie the age-associated increase in influenza  
8 mortality. *Mucosal Immunol* 12, 545-554.  
9  
10 Labat-Robert, J. (2004). Cell-matrix interactions in aging: role of receptors and matricryptins.  
11 *Ageing Res Rev* 3, 233-247.  
12  
13 Lämmermann, T., and Kastenmuller, W. (2019). Concepts of GPCR-controlled navigation in  
14 the immune system. *Immunol Rev* 289, 205-231.  
15  
16 Lopez-Otin, C., Blasco, M.A., Partridge, L., Serrano, M., and Kroemer, G. (2013). The  
17 hallmarks of aging. *Cell* 153, 1194-1217.  
18  
19 Lord, J.M., Midwinter, M.J., Chen, Y.F., Belli, A., Brohi, K., Kovacs, E.J., Koenderman, L.,  
20 Kubes, P., and Lilford, R.J. (2014). The systemic immune response to trauma: an overview of  
21 pathophysiology and treatment. *Lancet* 384, 1455-1465.  
22  
23 Mathias, J.R., Perrin, B.J., Liu, T.X., Kanki, J., Look, A.T., and Huttenlocher, A. (2006).  
24 Resolution of inflammation by retrograde chemotaxis of neutrophils in transgenic zebrafish. *J*  
25 *Leukoc Biol* 80, 1281-1288.  
26  
27 Minten, C., Alt, C., Gentner, M., Frei, E., Deutsch, U., Lyck, R., Schaeren-Wiemers, N., Rot,  
28 A., and Engelhardt, B. (2014). DARC shuttles inflammatory chemokines across the blood-  
29 brain barrier during autoimmune central nervous system inflammation. *Brain* 137, 1454-1469.  
30  
31 Ng, L.G., Ostuni, R., and Hidalgo, A. (2019). Heterogeneity of neutrophils. *Nat Rev Immunol*  
32 19, 255-265.  
33  
34 Nikolich-Zugich, J. (2018). The twilight of immunity: emerging concepts in aging of the immune  
35 system. *Nat Immunol* 19, 10-19.  
36  
37 Nomellini, V., Brubaker, A.L., Mahbub, S., Palmer, J.L., Gomez, C.R., and Kovacs, E.J.  
38 (2012). Dysregulation of neutrophil CXCR2 and pulmonary endothelial icam-1 promotes age-  
39 related pulmonary inflammation. *Ageing Dis* 3, 234-247.  
40  
41 Nomellini, V., Faunce, D.E., Gomez, C.R., and Kovacs, E.J. (2008). An age-associated  
42 increase in pulmonary inflammation after burn injury is abrogated by CXCR2 inhibition. *J*  
43 *Leukoc Biol* 83, 1493-1501.  
44  
45 Nourshargh, S., and Alon, R. (2014). Leukocyte migration into inflamed tissues. *Immunity* 41,  
46 694-707.  
47  
48 Novitzky-Basso, I., and Rot, A. (2012). Duffy antigen receptor for chemokines and its  
49 involvement in patterning and control of inflammatory chemokines. *Front Immunol* 3, 266.  
50  
51 Németh, T., Sperandio, M., and Mócsai, A. (2020). Neutrophils as emerging  
52 therapeutic targets. *Nat Rev Drug Discov* 19, 253-275.  
53

1 Oki, T., Kitaura, J., Eto, K., Lu, Y., Maeda-Yamamoto, M., Inagaki, N., Nagai, H., Yamanishi,  
2 Y., Nakajima, H., Nakajina, H., *et al.* (2006). Integrin alphaIIb beta3 induces the adhesion and  
3 activation of mast cells through interaction with fibrinogen. *J Immunol* 176, 52-60.  
4  
5 Owen-Woods, C., Joulia, R., Barkaway, A., Rolas, L., Ma, B., Nottebaum, A.F., Arkill, K.P.,  
6 Stein, M., Girbl, T., Golding, M., *et al.* (2020). Local microvascular leakage promotes trafficking  
7 of activated neutrophils to remote organs. *J Clin Invest* 130, 2301-2318.  
8  
9 Pilkington, S.M., Barron, M.J., Watson, R.E.B., Griffiths, C.E.M., and Bulfone-Paus, S. (2019).  
10 Aged human skin accumulates mast cells with altered functionality that localize to  
11 macrophages and vasoactive intestinal peptide-positive nerve fibres. *Br J Dermatol* 180, 849-  
12 858.  
13  
14 Pruenster, M., Mudde, L., Bombosi, P., Dimitrova, S., Zsak, M., Middleton, J., Richmond, A.,  
15 Graham, G.J., Segerer, S., Nibbs, R.J., and Rot, A. (2009). The Duffy antigen receptor for  
16 chemokines transports chemokines and supports their promigratory activity. *Nat Immunol* 10,  
17 101-108.  
18  
19 Raghuwanshi, S.K., Su, Y., Singh, V., Haynes, K., Richmond, A., and Richardson, R.M.  
20 (2012). The chemokine receptors CXCR1 and CXCR2 couple to distinct G protein-coupled  
21 receptor kinases to mediate and regulate leukocyte functions. *J Immunol* 189, 2824-2832.  
22  
23 Robba, C., Battaglini, D., Pelosi, P., and Rocco, P.R.M. (2020). Multiple organ dysfunction in  
24 SARS-CoV-2: MODS-CoV-2. *Expert Rev Respir Med*, 1-4.  
25  
26 Sapey, E., Greenwood, H., Walton, G., Mann, E., Love, A., Aaronson, N., Insall, R.H.,  
27 Stockley, R.A., and Lord, J.M. (2014). Phosphoinositide 3-kinase inhibition restores neutrophil  
28 accuracy in the elderly: toward targeted treatments for immunosenescence. *Blood* 123, 239-  
29 248.  
30  
31 Scapini, P., Marini, O., Tecchio, C., and Cassatella, M.A. (2016). Human neutrophils in the  
32 saga of cellular heterogeneity: insights and open questions. *Immunol Rev* 273, 48-60.  
33  
34 Shaw, A.C., Goldstein, D.R., and Montgomery, R.R. (2013). Age-dependent dysregulation of  
35 innate immunity. *Nat Rev Immunol* 13, 875-887.  
36  
37 Siebenhaar, F., Redegeld, F.A., Bischoff, S.C., Gibbs, B.F., and Maurer, M. (2018). Mast Cells  
38 as Drivers of Disease and Therapeutic Targets. *Trends Immunol* 39, 151-162.  
39  
40 Thiriot, A., Perdomo, C., Cheng, G., Novitzky-Basso, I., McArdle, S., Kishimoto, J.K., Barreiro,  
41 O., Mazo, I., Triboulet, R., Ley, K., *et al.* (2017). Differential DARC/ACKR1 expression  
42 distinguishes venular from non-venular endothelial cells in murine tissues. *BMC Biol* 15, 45.  
43  
44 Vabret, N., Britton, G.J., Gruber, C., Hegde, S., Kim, J., Kuksin, M., Levantovsky, R., Malle,  
45 L., Moreira, A., Park, M.D., *et al.* (2020). Immunology of COVID-19: Current State of the  
46 Science. *Immunity* 52, 910-941.  
47  
48 Voehringer, D., Liang, H.E., and Locksley, R.M. (2008). Homeostasis and effector function of  
49 lymphopenia-induced "memory-like" T cells in constitutively T cell-depleted mice. *J Immunol*  
50 180, 4742-4753.  
51  
52 Wang, J., Hossain, M., Thanabalasuriar, A., Gunzer, M., Meininger, C., and Kubes, P. (2017).  
53 Visualizing the function and fate of neutrophils in sterile injury and repair. *Science* 358, 111-  
54 116.  
55

1 Weninger, W., Biro, M., and Jain, R. (2014). Leukocyte migration in the interstitial space of  
2 non-lymphoid organs. *Nat Rev Immunol* 14, 232-246.  
3  
4 Woodfin, A., Voisin, M.B., Beyrau, M., Colom, B., Caille, D., Diapouli, F.M., Nash, G.B.,  
5 Chavakis, T., Albelda, S.M., Rainger, G.E., *et al.* (2011). The junctional adhesion molecule  
6 JAM-C regulates polarized transendothelial migration of neutrophils in vivo. *Nat Immunol* 12,  
7 761-769.  
8  
9 Wulfert, F.M., van Meurs, M., Kurniati, N.F., Jongman, R.M., Houwertjes, M.C., Heeringa, P.,  
10 Struys, M.M., Zijlstra, J.G., and Molema, G. (2012). Age-dependent role of microvascular  
11 endothelial and polymorphonuclear cells in lipopolysaccharide-induced acute kidney injury.  
12 *Anesthesiology* 117, 126-136.  
13

## Key Resources Tables

REAGENT or RESOURCE	SOURCE	IDENTIFIER
Antibodies		
Anti-mouse ACKR1 (clone 6B7)	(Thiriot et al., 2017)	NA
Anti-mouse CD117 (c-Kit) Alexa Fluor 647 (Clone 2B8)	Biolegend	Cat#105818; RRID: AB_493474
Anti-mouse CD117 (c-Kit) APC (Clone 2B8)	Biolegend	Cat#123121; RRID: AB_313220
Anti-mouse CD16/32 Purified Antibody	Biolegend	Cat#101301 ; RRID: AB_312800
Anti-mouse CD182 (CXCR2) PE (Clone SA044G4)	Biolegend	Cat#149303 ; RRID: AB_2565691
Anti-mouse CD184 (CXCR4) Monoclonal Antibody (2B11), PerCP-eFluor 710	Thermo Fischer Scientific	Cat#46-9991-80 ; RRID: AB_10670489
Anti-mouse CD31 (clone 390)	Thermo Fischer Scientific	Cat#16-0311-85 RRID: AB_468933
Anti-mouse CD45 Pacific Blue (clone 30-F11)	Biolegend	Cat#103126; RRID: AB_493535
Anti-mouse CD54 PE/Cy7 (Clone YN1/1.7.4)	Biolegend	Cat#116121 ; RRID: AB_2715949
Anti-mouse CD62L Brilliant Violet 605 (Clone MEL-14)	Biolegend	Cat#104437 ; RRID: AB_11125577
Anti-mouse c-Kit (CD117) (clone D13A2)	Cell Signalling Technology	Cat#3074T; RRID: AB_1147633
Anti-mouse CXCL1 (polyclonal)	R&D systems	Cat#AF-453-NA; RRID: AB_354495
Anti-mouse CXCR2 Alexa Fluor 647 (clone SA044G4)	Biolegend	Cat#149305; RRID: AB_2565693
Anti-mouse F4/80 Alexa Fluor 647 (Clone BM8)	Biolegend	Cat#123121; RRID: AB_893492
Anti-mouse FcεR1α Pacific Blue (Clone MAR1)	Biolegend	Cat#134313; RRID: AB_10612933
Anti-mouse GRK2	Genetex	Cat# GTX101682
Anti-mouse Ly6G Pacific Blue™ (Clone 1A8)	Biolegend	Cat# 127611 RRID: AB_1877212
Anti-mouse Ly6G Alexa Fluor 488 (Clone 1A8)	Biolegend	Cat#127625 ; RRID: AB_1186108
Anti-mouse Ly6G Alexa Fluor 647 (clone 1A8)	Biolegend	Cat#127610; RRID: AB_1134159
Anti-mouse Ly6G Biotin (Clone 1A8)	Biolegend	Cat#127604; RRID: AB_2561339
Anti-mouse MRP14 (clone 2B10)	Gift from Dr N.Hogg (Francis Crick Institute, UK)	NA
Anti-mouse/human CD11b Brilliant Violet 711 (Clone M1/70)	Biolegend	Cat#101241 ; RRID: AB_11218791
Anti-mouse/rat CD29 PE/Cy7 (Clone HMβ1-1)	Biolegend	Cat#102221 ; RRID: AB_528789
Anti-mouse CD206 Alexa Fluor 647 (clone C068C2)	Biolegend	Cat#141711 ; AB_10900240
Anti-Neutrophil Elastase antibody	Abcam	Cat#ab68672 ; RRID: AB_1658868

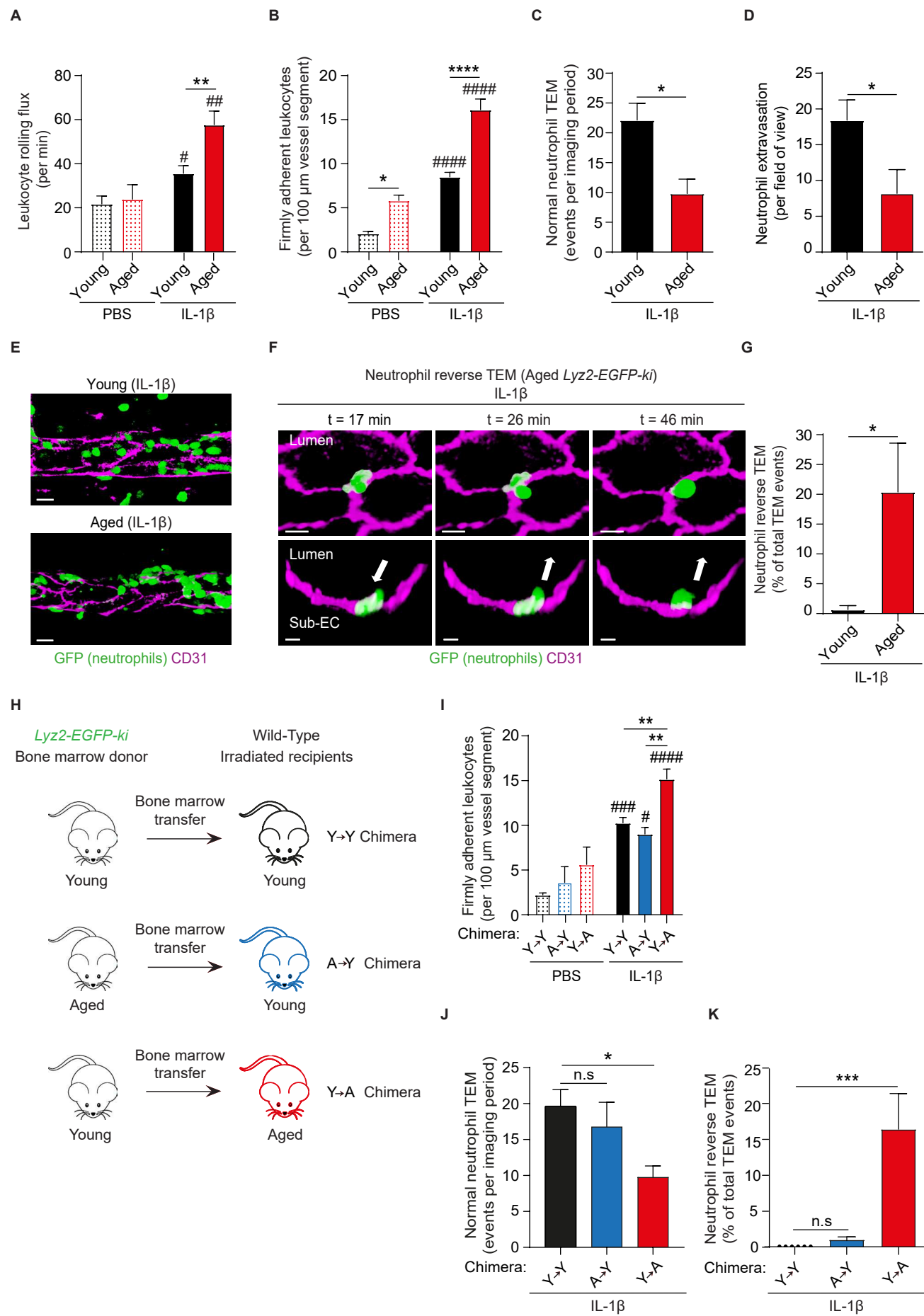
Armenian Hamster IgG Isotype Ctrl PE/Cy7	Biolegend	Cat#400921
Blocking anti-mouse CXCL1 (clone 48415)	R&D systems	Cat#MAB453; RRID: AB_2087696
Blocking anti-mouse CXCL2 (clone 40605)	R&D systems	Cat#MAB452; RRID: AB_2230058
Blocking anti-mouse IgG2a	Biolegend	NA
Depletion Anti-mouse CD117 (c-kit) Antibody Ultra-LEAF™ Purified (Clone ACK2)	Biolegend	Cat#135131 ; RRID: AB_2571992
Depletion Anti-mouse IgG2b κ Isotype control (Clone ACK2)	Biolegend	Cat# 135131; RRID 2571992
Polyclonal goat anti-rabbit immunoglobulins/HRP conjugated antibody	Agilent/Dako	Cat#P044801-2
Rat IgG2a, κ Isotype Ctrl PE (Clone RTK2758)	Biolegend	Cat#400507
Rat IgG2b kappa Isotype Control (eB149/10H5), PerCP-eFluor 710	Thermo Fisher Scientific	Cat#46-4031-80 ; RRID: AB_1834457
Rat IgG2b, κ Isotype Ctrl Antibody Brilliant Violet 711 (Clone RTK4530)	Biolegend	Cat#400653
Biological Samples		
Bone marrow: mouse <i>Mrp8-Cre;Grk2<sup>fl</sup>;Lyz2-EGFP-ki</i>	Dr Tim Lämmermann (Max Planck Institute of Immunobiology and Epigenetics, Germany)	NA
Critical commercial assay		
Alexa Fluor 488 antibody labeling kit	Thermo Fisher Scientific	Cat# A20181
Alexa Fluor 555 antibody labeling kit	Thermo Fisher Scientific	Cat#A20187
Alexa Fluor 647 antibody labeling kit	Thermo Fisher Scientific	Cat#A20186
Anti-Ly-6G MicroBeads UltraPure, mouse	Milteny biotech	Cat# 130-120-337
DyLight 405 antibody labeling kit	Thermo Fisher Scientific	Cat#53021
Mouse CXCL1/KC DuoSet ELISA	R&D Systems	Cat#453-05
Proteome Profiler Mouse Cytokine Array Kit, Panel A	R&D Systems	Cat#ARY006
Chemicals, Peptides, and Recombinant Proteins		
AF647-streptavidin	Thermo Fisher Scientific	Cat#S21374
Avidin, Alexa Fluor 488 conjugate	Thermo Fischer Scientific	Cat# A21370
Avidin, Egg White	Thermo Fisher Scientific	Cat#A2667
Bafilomycin	AlfaAesar	Cat#J67193
BSA, low endotoxin	Sigma-Aldrich	Cat#A9543
C12FDG (5-Dodecanoylaminofluorescein Di-β-D-Galactopyranoside)	Thermo Fischer Scientific	Cat#D2893

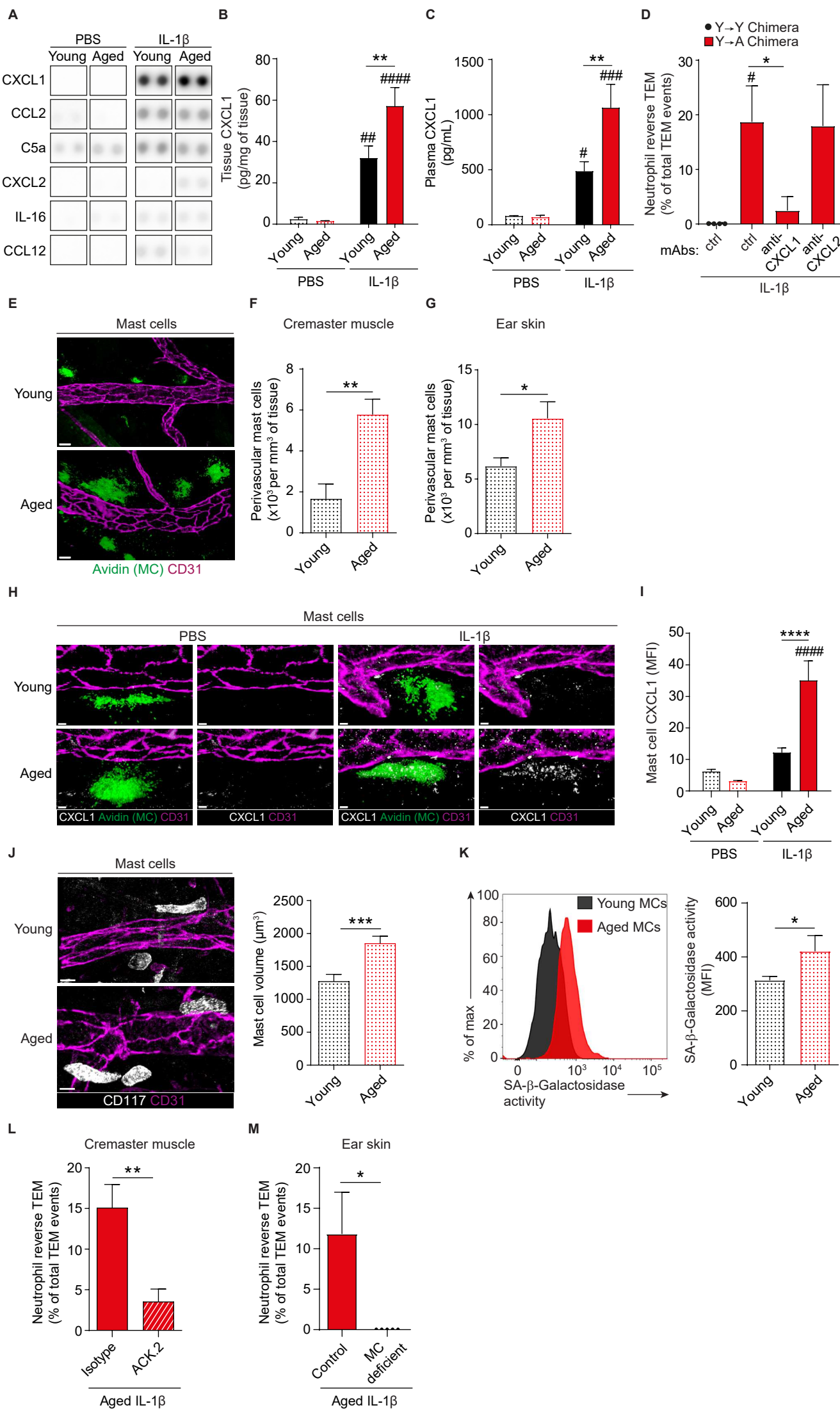
DAPI (4',6-Diamidino-2-Phenylindole, Dilactate)	Biolegend	Cat#422801
Evans Blue	Sigma	Cat#E2129
FITC Annexin V	BD	Cat#560931
Halt Protease and Phosphatase Inhibitor Cocktail (100X)	Thermo Fisher Scientific	Cat#78440
Propidium iodide solution	Biolegend	Cat#421301
Recombinant murine IL-1 $\beta$	R&D Systems	Cat#401-ML-005/CF
Recombinant murine TNF- $\alpha$ aa 80-235	R&D Systems	Cat#410-MT-010/CF
Triton X-100	Sigma	Cat#T8787-100ML
Experimental Models: Organisms/Strains		
Mouse, <i>Ackr1<sup>-/-</sup></i>	(Dawson et al., 2000)	NA
Mouse C57BL/6	Charles River laboratories	JAX 000664
Mouse, C57BL/6JRj	Janvier laboratories	Cat#SC-C57J-M
Mouse, <i>Lyz2-EGFP-ki</i>	Gift from Dr M. Sperandio (Ludwig Maximilians University Munich, Germany) (Faust et al., 2000)	NA
Mouse, <i>Mcpt5-Cre-R-DTA</i>	Provided by Prof. Axel Roers (Medical Faculty Carl Gustav Carus, Technische Universität Dresden)	NA
Software and Algorithms		
FlowJo v10	Tree Star	<a href="https://www.flowjo.com/">https://www.flowjo.com/</a>
ImageJ	Wayne Rasband (NIH)	<a href="https://imagej.nih.gov/ij/">https://imagej.nih.gov/ij/</a>
Imaris v9	Bitplane	<a href="https://imaris.oxinst.com/packages">https://imaris.oxinst.com/packages</a>
Prism v8	Graphpad	<a href="https://www.graphpad.com/scientific-software/prism/">https://www.graphpad.com/scientific-software/prism/</a>
Other		
123 eBeads™ counting beads	Thermo Fisher Scientific	Cat#01-1234-42
FluoSpheres™; Carboxylate-Modified Microspheres, 0.02 $\mu$ m, red fluorescent (580/605)	Invitrogen	Cat#F8786
Latex-Free Orthodontic Elastic Bands	Dental Aesthetics	Cat#UNL735-F

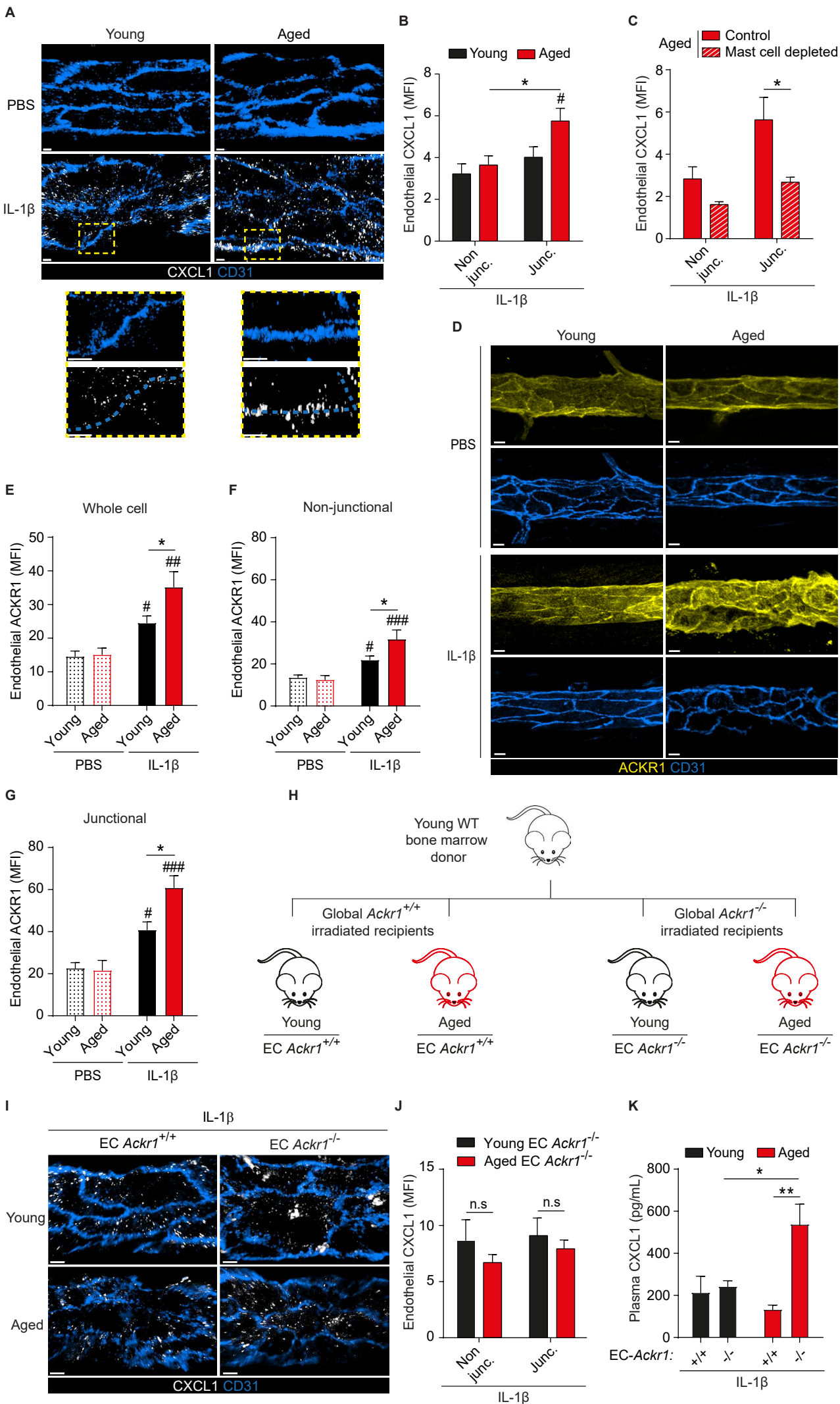


UltraComp eBeads™ Compensation Beads	ThermoFisher Scientific	Cat#01-2222-42
Zombie Yellow™ Fixable Viability Kit	Biolegend	Cat#423103

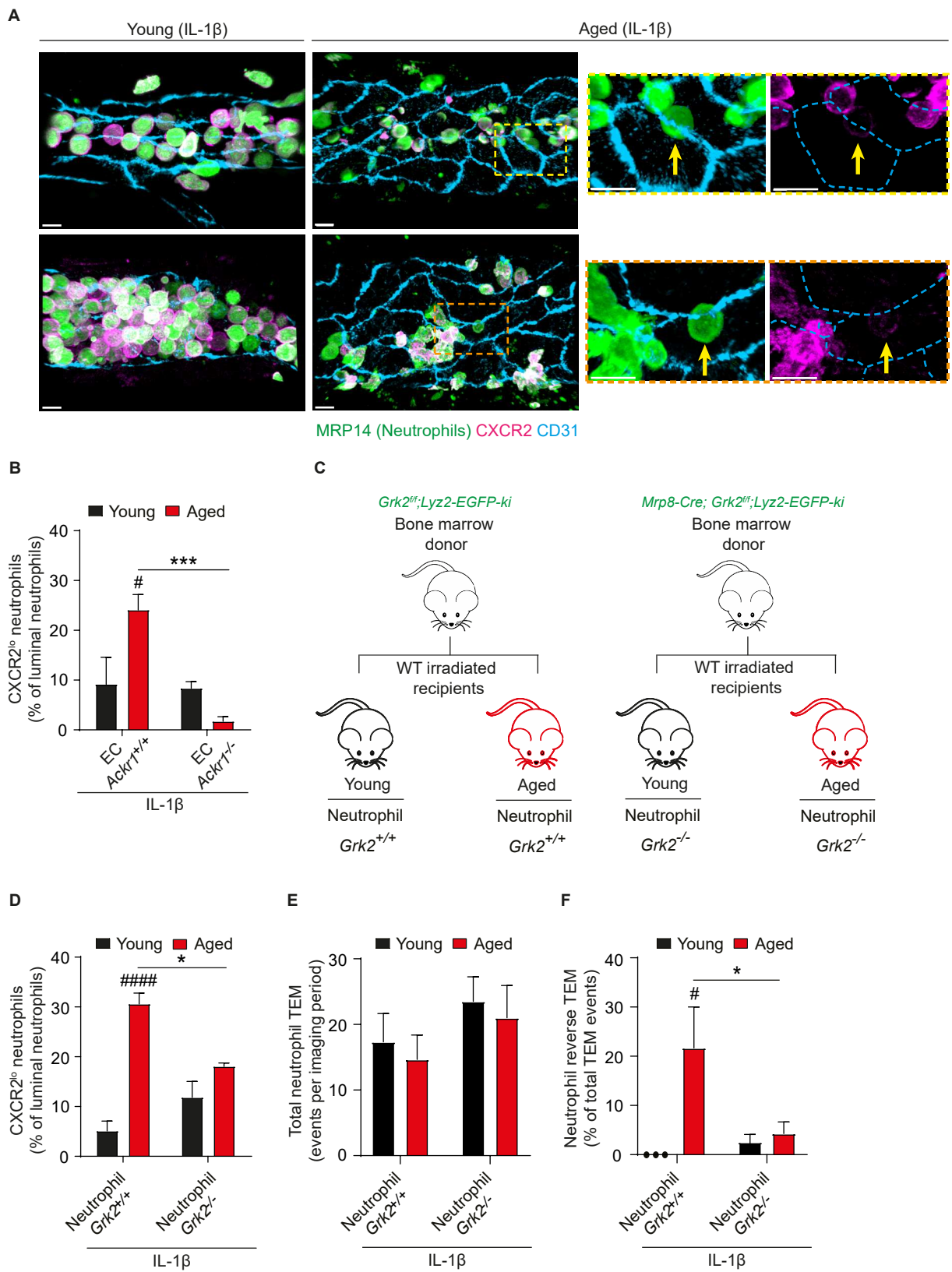
**Figure 1**

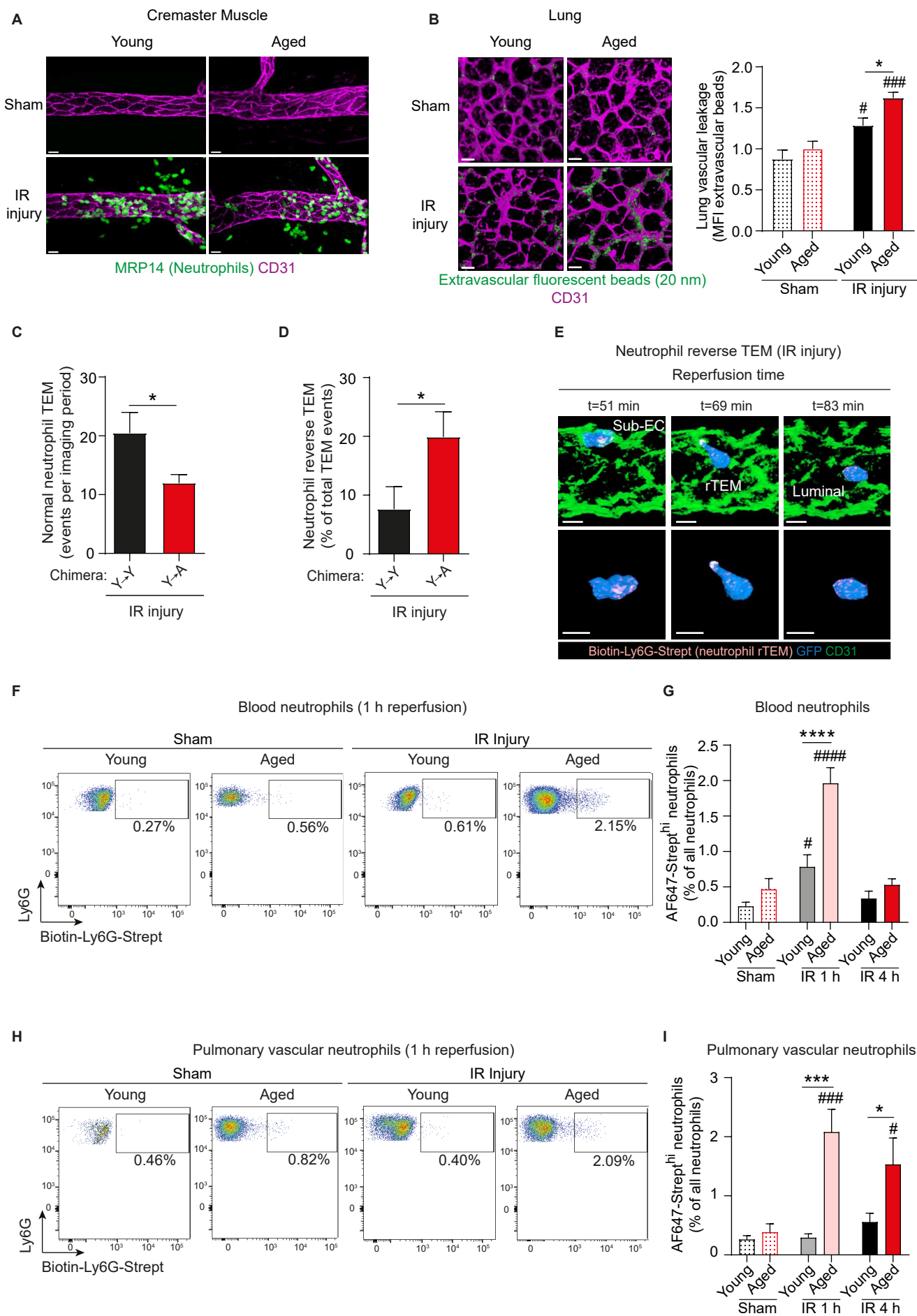


**Figure 2**

**Figure 3**

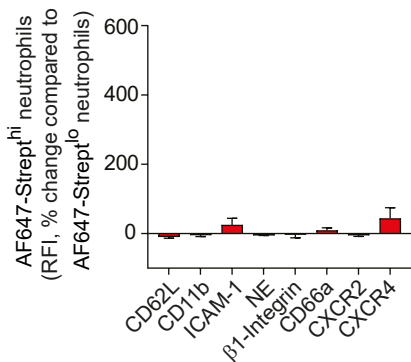
**Figure 4**



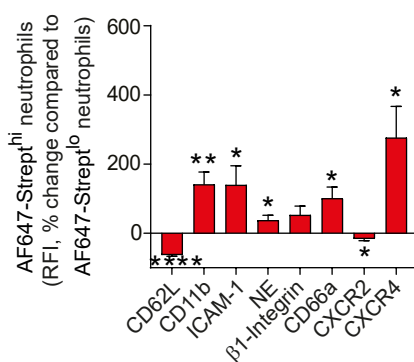
**Figure 5**

**Figure 6****A**

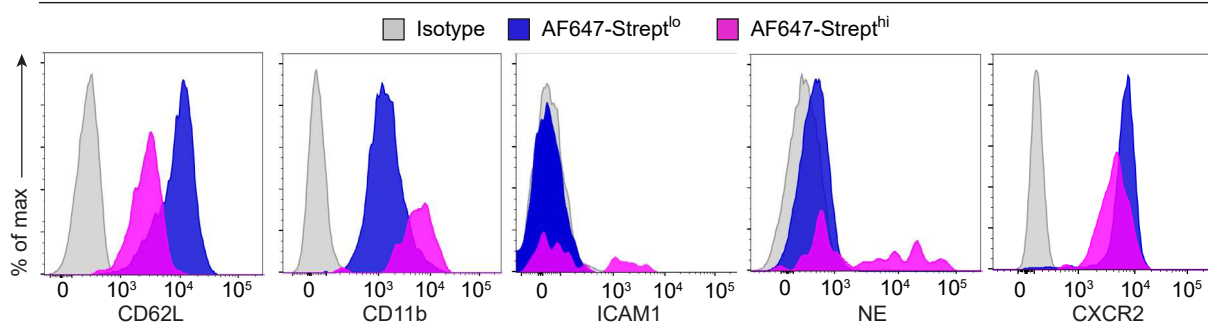
Pulmonary vascular neutrophils  
Aged: IR injury 1 h reperfusion

**B**

Pulmonary vascular neutrophils  
Aged: IR injury 4 h reperfusion

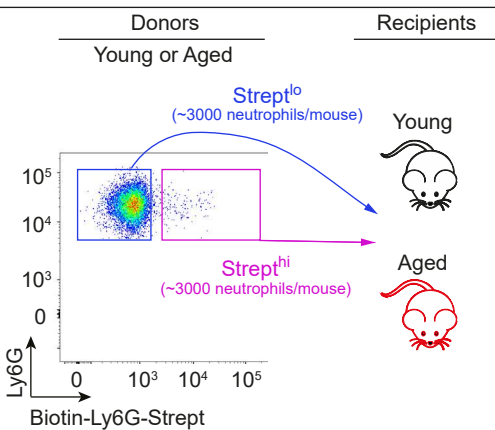
**C**

Pulmonary vascular neutrophils  
(Aged: IR injury, 4 h reperfusion)

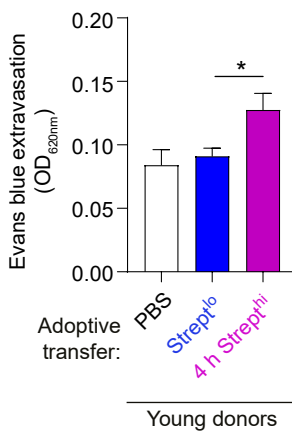
**D**

Young or aged donors subjected to IR injury:

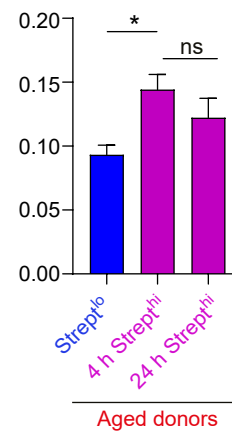
AF647 Strept<sup>hi</sup> and AF647 Strept<sup>lo</sup> blood neutrophils sorted and injected i.v. into naive young or aged recipients

**E**

Aged recipients:  
Lung permeability

**F**

Aged recipients:  
Lung permeability

**G**

Young recipients:  
Lung permeability

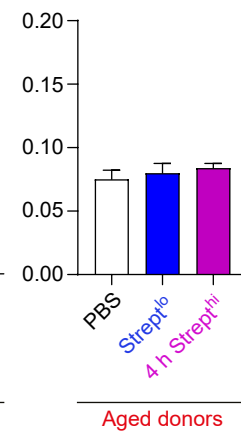


**Figure 7**

**A**

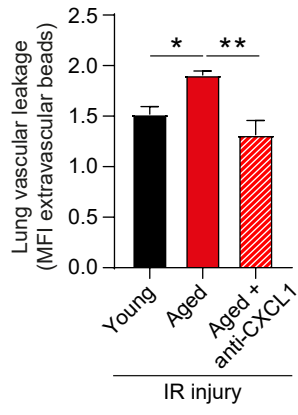
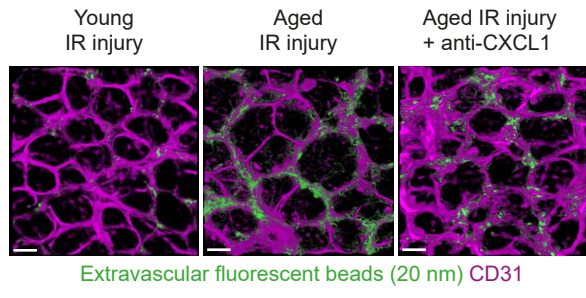
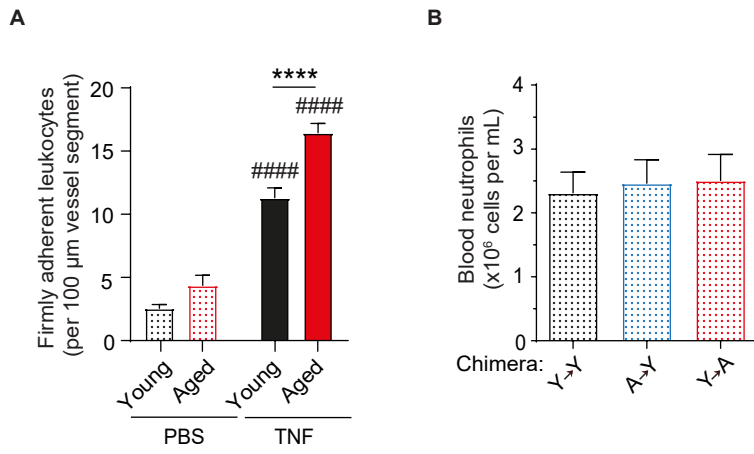


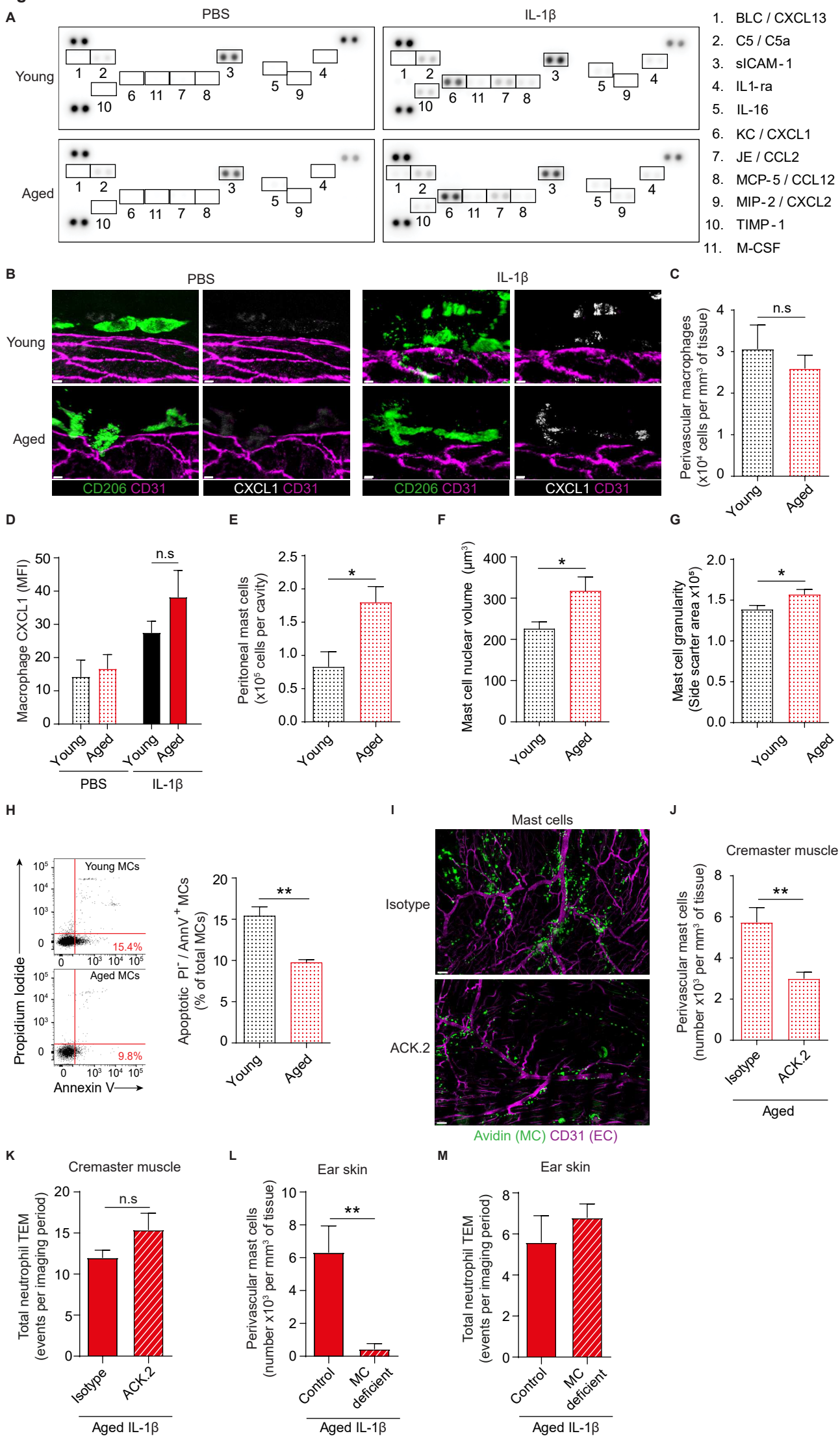


Figure S1

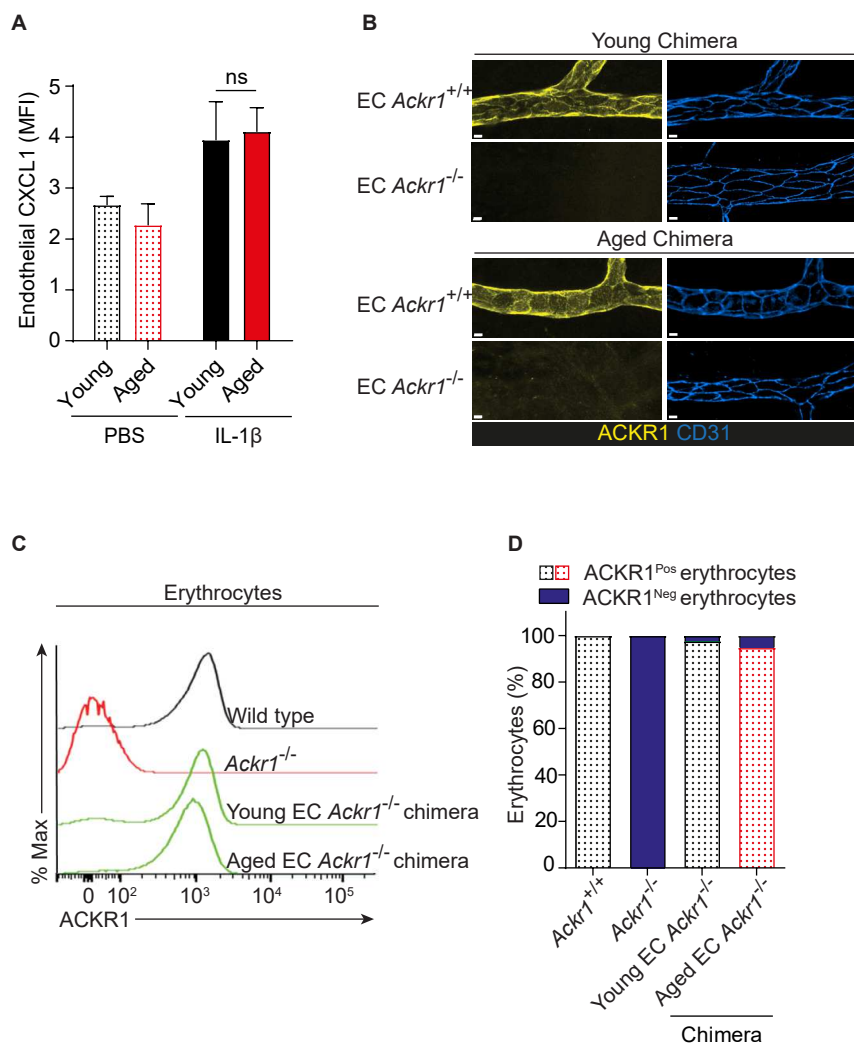


**Figure S1 (Related to Figure 1). Leukocyte adhesion responses in TNF-stimulated venules of WT mice and chimeric mice characterization. (A)** Young (2-4 months) and aged ( $\geq 18$  months) mice were treated intrascrotally (i.s.) with PBS or TNF and leukocyte firm adhesion in cremasteric post-capillary venules quantified by brightfield IVM ( $n=3-7$  mice/group). **(B)** Total neutrophil blood counts in chimeric mice (as generated in Figure 1H) at 4 weeks post irradiation and bone marrow transfer ( $n \geq 10$  mice/group). Means  $\pm$  SEM, #### $p < 0.0001$  as compared to age-matched controls, \*\*\*\* $p < 0.0001$  as indicated.

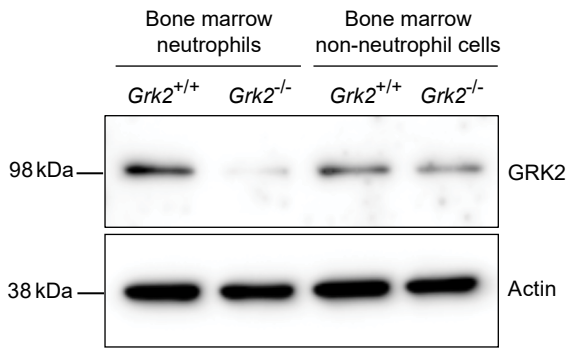
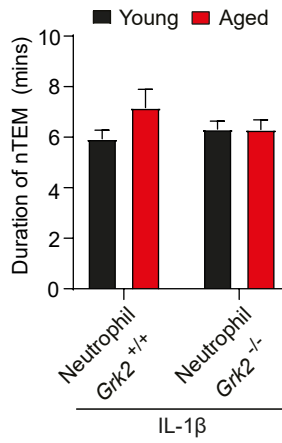
**Figure S2**



**Figure S2 (Related to Figure 2). Characterization of pro-inflammatory mediator generation and stromal cells in young and aged stimulated cremasteric tissues. (A-D)** Young and aged WT mice were stimulated i.s. with IL-1 $\beta$  or PBS for 4 h. **(A)** Inflammatory mediator detection by protein array in cremaster muscles (n=3 mice/condition). **(B)** Representative confocal images depicting CXCL1 expression by perivascular macrophages (CD206; scale bar: 5  $\mu$ m), **(C)** macrophage numbers associated with post-capillary venules and **(D)** immunoreactive CXCL1 expression (MFI) in these cells (n=4-6 mice/group). **(E)** Number of peritoneal mast cells (MCs) in naïve young and aged WT mice as assessed by flow cytometry (n=3-5 mice/group). **(F)** Quantification of MC nuclear volume in un-stimulated ear skins as assessed by confocal microscopy (n=3 mice/group). Peritoneal MCs acquired from un-stimulated young and aged mice assayed for **(G)** granularity (n=5 mice/group) and **(H)** apoptosis (n=6-7 mice/group), both by flow cytometry. **(I-K)** Aged WT mice were treated with anti-CD117 (ACK.2) mAb or isotype control for mast cell (MC) depletion. **(I)** Representative tile scan confocal images of the cremaster muscle microcirculation (scale bar: 300  $\mu$ m), **(J)** quantification of MCs (avidin) associated with post-capillary venules (CD31) (n=3-5 mice/group) and **(K)** total neutrophil TEM events in IL-1 $\beta$ -stimulated control or mast cell depleted aged mice. **(L)** Quantification of MC numbers associated with post-capillary venules in ear skins stained with avidin (MCs) and anti-CD31 mAb (ECs) and **(M)** total neutrophil TEM events in IL-1 $\beta$ -stimulated ear skin of MC deficient (*Mcpt5-Cre-R-DTA*) aged mice and their littermate controls (n=5-7 mice/group). Means  $\pm$  SEM, \*p<0.05, \*\*p<0.01, n.s. not significant as indicated.

**Figure S3**

**Figure S3 (Related to Figure 3) EC CXCL1 expression and EC *Acker1*<sup>-/-</sup> chimeric mice characterization.** (A) EC CXCL1 quantification (MFI) in young and aged mouse cremasteric post capillary venules (PCVs) treated with PBS or IL-1 $\beta$  (n = 6-7 mice/group). (B) Representative confocal images of ear skin PCVs immunostained for ACKR1 and CD31 from young and aged EC *Acker1*<sup>+/+</sup> and EC *Acker1*<sup>-/-</sup> chimeric mice (scale bar: 20  $\mu$ m). (C) Flow cytometry analysis of erythrocyte (Ter119<sup>+</sup>) ACKR1 expression and (D) relative percentages of ACKR1<sup>+</sup> and ACKR1<sup>-</sup> erythrocytes in peripheral blood of chimeric mice generated as described in Figure 3H (n=3-4 mice/group). Means  $\pm$  SEM, n.s. not significant as indicated.

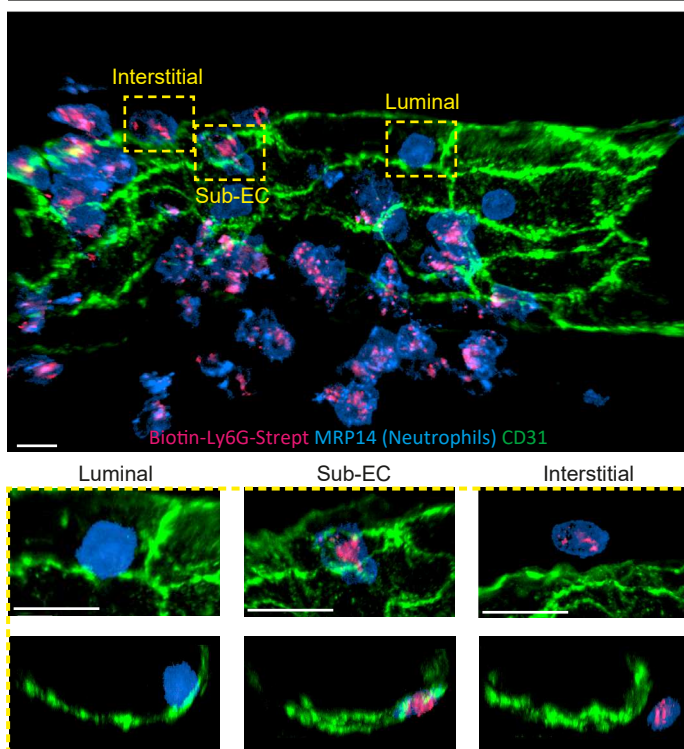
**Figure S4****A****B**

**Figure S4 (Related to Figure 4). Validation of neutrophil GRK2 deficiency and analysis of neutrophil TEM duration.** (A) GRK2 expression in purified bone marrow derived neutrophils and non-neutrophil cells of neutrophil *Grk2*<sup>+/+</sup> and *Grk2*<sup>-/-</sup> chimeric mice as analyzed by western blot (loading control: Actin). (B) Duration of neutrophil normal TEM (mins) as assessed by confocal IVM in IL-1 $\beta$ -stimulated cremaster muscles of young and aged neutrophil *Grk2*<sup>+/+</sup> and *Grk2*<sup>-/-</sup> chimeric mice (n=30-82 neutrophils analyzed/group). Means  $\pm$  SEM.

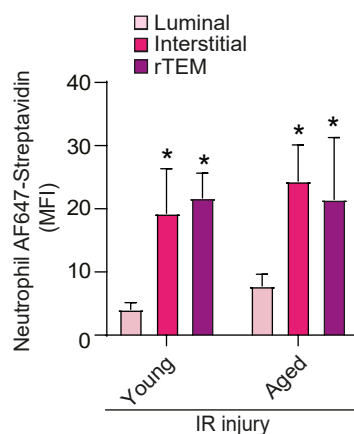
Figure S5

A

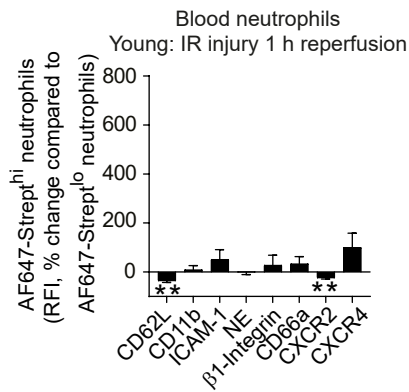
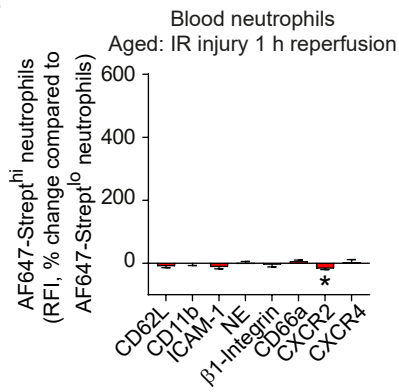
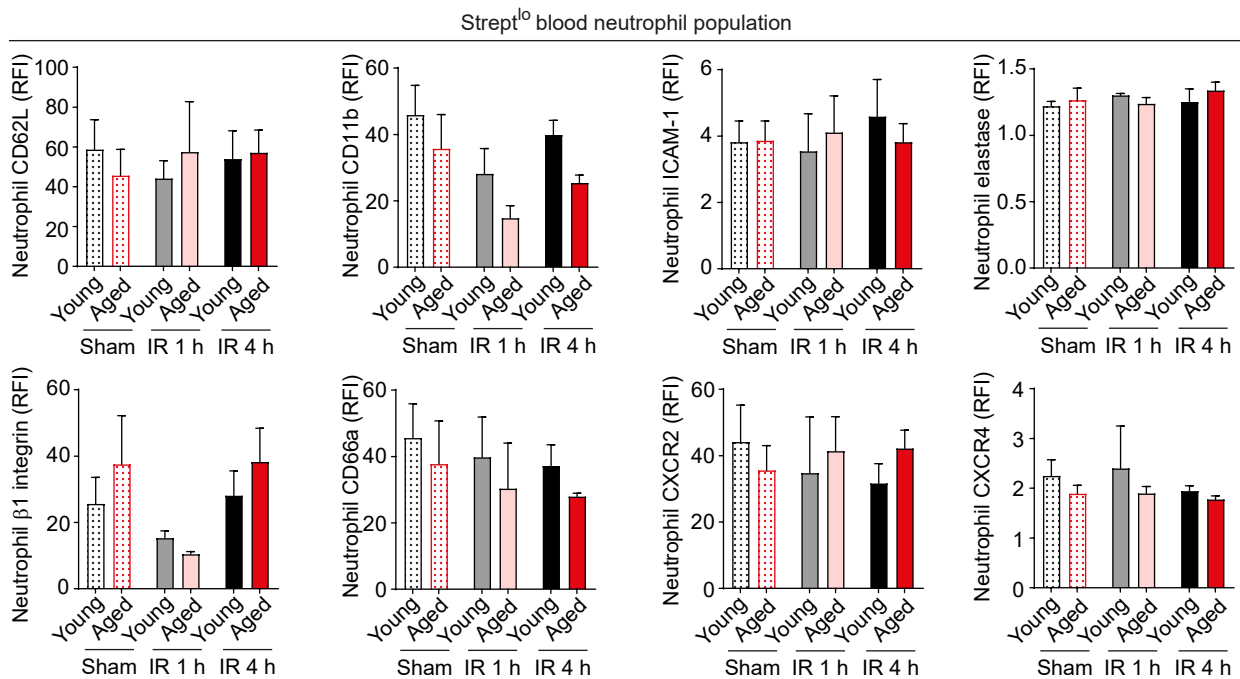
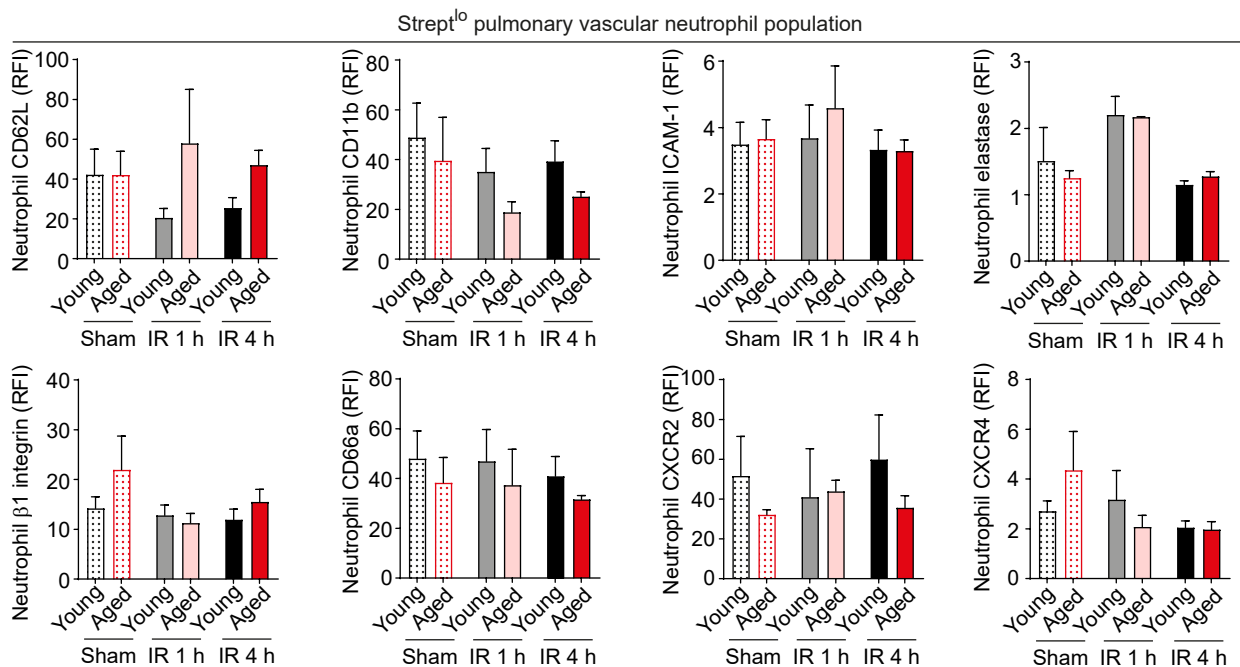
Aged IR injury



B



**Figure S5 (Related to Figure 5). Validation of biotin-Ly6G-AF647-Streptavidin cell tracking, as a method for specifically labelling neutrophils that have breached the endothelium.** Young and aged WT mice were injected i.v. with biotinylated anti-Ly6G mAb, subjected to sham or cremasteric IR injury and AF647-Strept was applied locally to cremaster muscles. **(A)** Representative confocal images of neutrophil AF647-Strept signal in the vascular lumen, subendothelial space and interstitium during IR injury in aged WT mice (dashed boxes delineate magnified areas; scale bar: 10 μm). **(B)** AF647-Strept quantification (MFI) of neutrophils within the lumen, interstitial tissue, and cells undergoing rTEM in IR-stimulated cremaster muscles of young and aged *Lyz2-EGFP-ki* mice (n=3-4 mice/group). Means ± SEM \* p<0.05 as compared to MFI of age-matched luminal neutrophils.

**Figure S6****A****B****C****D**

**Figure S6 (Related to Figure 6). Phenotypic analysis of AF647-Strept<sup>lo</sup> and AF647-Strept<sup>hi</sup> blood and pulmonary vascular neutrophils.** Young and aged WT mice were injected i.v. with biotinylated anti-Ly6G mAb, subjected to sham or cremasteric IR injury and AF647-Strept was applied locally to cremaster muscles. Relative expression levels of indicated markers on AF647-Strept<sup>hi</sup> neutrophils relative to levels on AF647-Strept<sup>lo</sup> neutrophils in the blood following 1 h reperfusion in **(A)** young and **(B)** aged IR-stimulated mice. Relative expression of indicated markers on AF647-Strept<sup>lo</sup> **(C)** blood neutrophils and **(D)** neutrophils from the pulmonary vasculature (n=5 mice/group). Means  $\pm$  SEM \*p<0.05, \*\*p<0.01 as compared to AF647-Strept<sup>lo</sup> neutrophils of the same group.



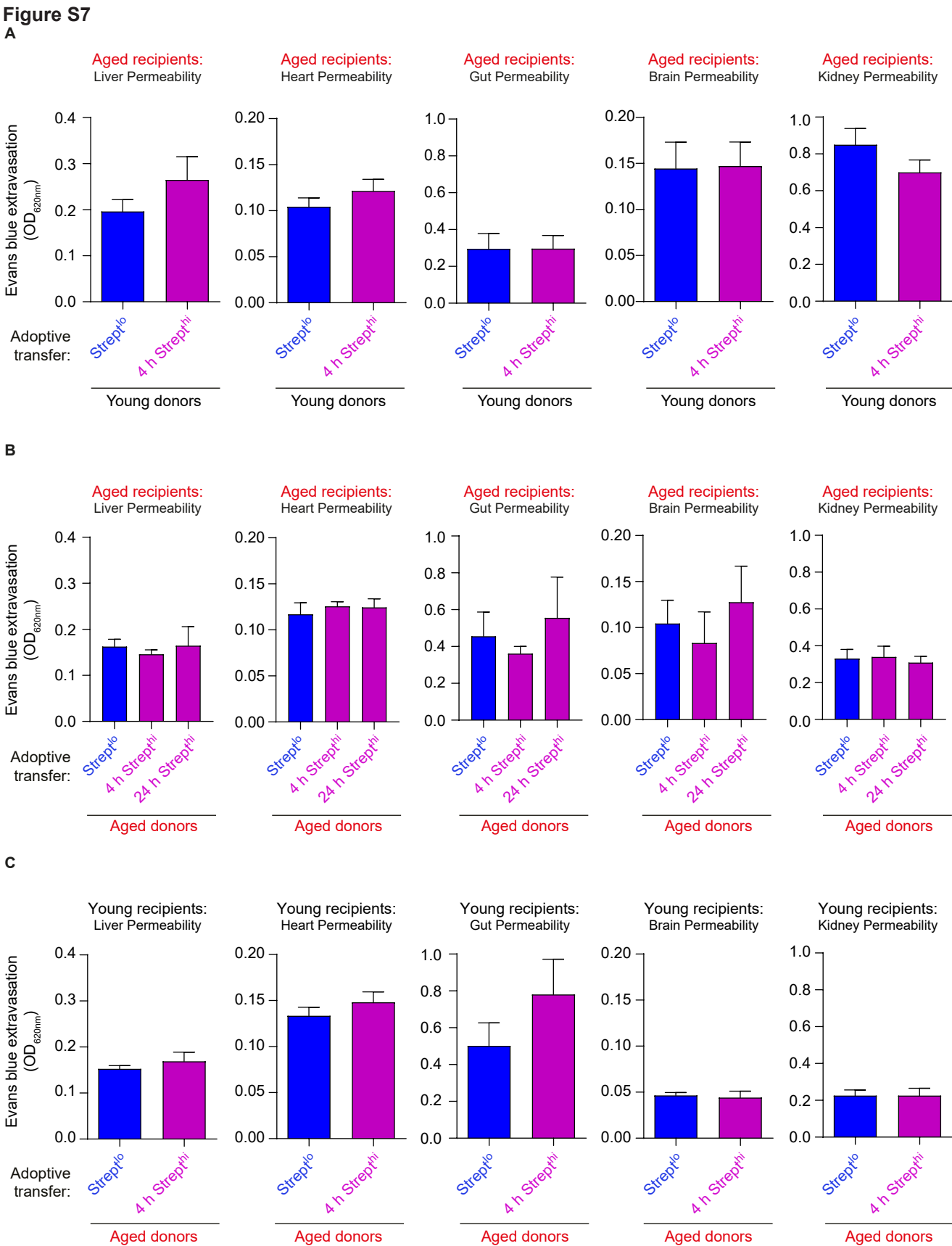
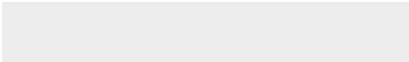
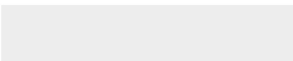


**Figure S7 (Related to Figure 6). Impact of AF647-Strept<sup>lo</sup> and AF647-Strept<sup>hi</sup> neutrophils on organ permeability.** Extravasation of i.v. Evans blue in multiple tissues of (A) aged recipients 4 h post i.v. injection of neutrophils sorted from young donors, (B) aged recipients 4 or 24 h post i.v. injection of neutrophils sorted from aged donors, and (C) young recipients 4 h post i.v. injection of neutrophils sorted from aged donors (n=4-7 mice/group). Means ± SEM.



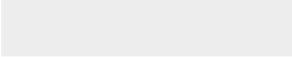
[Click here to access/download](#)

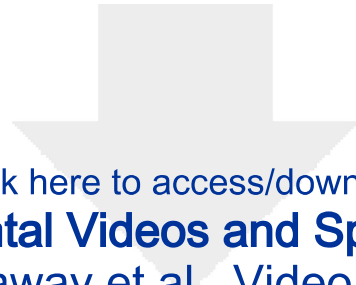
**Supplemental Videos and Spreadsheets**  
A Barkaway et al., Video S1.mp4





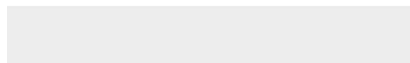
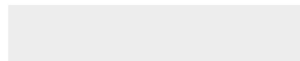
[Click here to access/download](#)  
**Supplemental Videos and Spreadsheets**  
A Barkaway et al., Video S2.mp4





[Click here to access/download](#)

**Supplemental Videos and Spreadsheets**  
A Barkaway et al., Video S3.mp4

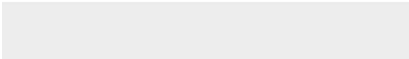
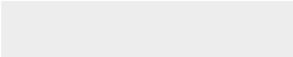


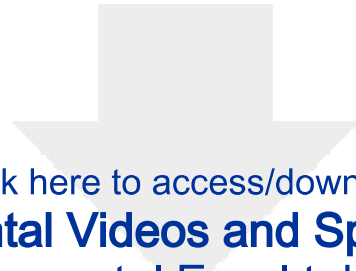


[Click here to access/download](#)

**Supplemental Videos and Spreadsheets**

A Barkaway et al., Video S4 hi.mp4





[Click here to access/download](#)

**Supplemental Videos and Spreadsheets**  
A Supplemental Excel table 1.xlsx

